JBC RESEARCH ARTICLE

RGS14 regulates PTH- and FGF23-sensitive NPT2A-mediated renal phosphate uptake *via* binding to the NHERF1 scaffolding protein

Received for publication, December 23, 2021, and in revised form, March 4, 2022 Published, Papers in Press, March 17, 2022,
https://doi.org/10.1016/j.jbc.2022.101836

Peter A. Friedman[1,2,*], W. Bruce Sneddon[1], Tatyana Mamonova[1], Carolina Montanez-Miranda[3], Suneela Ramineni[3], Nicholas H. Harbin[3], Katherine E. Squires[3], Julia V. Gefter[1], Clara E. Magyar[4], David R. Emlet[5], and John R. Hepler[3,*]

From the [1]Laboratory for GPCR Biology, Department of Pharmacology and Chemical Biology, and [2]Department of Structural Biology, University of Pittsburgh School of Medicine, Pittsburgh, Pennsylvania, USA; [3]Department of Pharmacology and Chemical Biology, Emory University School of Medicine, Atlanta, Georgia, USA; [4]Department of Pathology and Laboratory Medicine, The David Geffen School of Medicine at UCLA, Los Angeles, California, USA; [5]Center for Critical Care Nephrology, Department of Critical Care Medicine, University of Pittsburgh School of Medicine, Pittsburgh, Pennsylvania, USA

Edited by Roger Colbran

Phosphate homeostasis, mediated by dietary intake, renal absorption, and bone deposition, is incompletely understood because of the uncharacterized roles of numerous implicated protein factors. Here, we identified a novel role for one such element, regulator of G protein signaling 14 (RGS14), suggested by genome-wide association studies to associate with dysregulated Pi levels. We show that human RGS14 possesses a carboxy-terminal PDZ ligand required for sodium phosphate cotransporter 2a (NPT2A) and sodium hydrogen exchanger regulatory factor-1 (NHERF1)–mediated renal Pi transport. In addition, we found using isotope uptake measurements combined with bioluminescence resonance energy transfer assays, siRNA knockdown, pull-down and overlay assays, and molecular modeling that secreted proteins parathyroid hormone (PTH) and fibroblast growth factor 23 inhibited Pi uptake by inducing dissociation of the NPT2A–NHERF1 complex. PTH failed to affect Pi transport in cells expressing RGS14, suggesting that it suppresses hormone-sensitive but not basal Pi uptake. Interestingly, RGS14 did not affect PTH-directed G protein activation or cAMP formation, implying a postreceptor site of action. Further pull-down experiments and direct binding assays indicated that NPT2A and RGS14 bind distinct PDZ domains on NHERF1. We showed that RGS14 expression in human renal proximal tubule epithelial cells blocked the effects of PTH and fibroblast growth factor 23 and stabilized the NPT2A–NHERF1 complex. In contrast, RGS14 genetic variants bearing mutations in the PDZ ligand disrupted RGS14 binding to NHERF1 and subsequent PTH-sensitive Pi transport. In conclusion, these findings identify RGS14 as a novel regulator of hormone-sensitive Pi transport. The results suggest that changes in RGS14 function or abundance may contribute to the hormone resistance and hyperphosphatemia observed in kidney diseases.

Parathyroid hormone (PTH) and fibroblast growth factor 23 (FGF23) control serum Pi levels by inhibiting the sodium phosphate cotransporter 2a (NPT2A) in the kidney, thereby promoting regulated Pi excretion. Hormonal control of this process requires the PDZ scaffold protein sodium hydrogen exchanger regulatory factor-1 (NHERF1) (1). Mice lacking NHERF1 and humans harboring NHERF1 mutations are hypophosphatemic, consequent to urinary Pi loss, and osteopenia because of insufficient serum Pi reserves. The cognate type 1 PTH G protein–coupled receptor (PTHR) mediates PTH actions, whereas FGF23 operates through the FGF receptor 1 (FGFR1) receptor tyrosine kinase. Though the two hormones act through structurally unrelated receptor forms, PTH and FGF23 initiate signaling pathways that converge on the NPT2A–NHERF1 complex in kidney cells to inhibit Pi uptake. In the absence of NHERF1, Pi excretion continues unabated with attendant loss of PTH and FGF23 regulation.

Despite advances in understanding the biochemical events underlying this process, critical gaps exist in our knowledge of hormone regulatory actions because of additional unidentified components. Here, we introduce evidence that regulator of G protein signaling 14 (RGS14) is one such factor. Numerous genome-wide association studies (GWASs) implicate RGS14 in kidney diseases (2–7), including disordered Pi metabolism. The *RGS14* gene on human chromosome 5 is adjacent to *SLC34A1*, which encodes NPT2A. Coding mutations have been identified (8) in the human RGS14 PDZ-binding motif, as we reported (9), though the impact of these variants on RGS14 function is unknown. Potential interactions and functional consequences of RGS14 engagement of PDZ proteins have not been described.

RGSs are GTPase-activating proteins that function primarily as central components of G protein–coupled receptor and G protein signaling pathways (10, 11). RGS14 is an unusual multifunctional scaffolding protein that integrates G protein, mitogen-activated protein kinase, and Ca^{2+}/calmodulin signaling pathways (12, 13). It is the only RGS protein that

* For correspondence: Peter A. Friedman, paf10@pitt.edu; John R. Hepler, jhepler@emory.edu.

harbors a canonical PDZ-recognition motif. Rgs14[1] is most highly expressed in rodents in the brain, lung, heart, and spleen (14). Rgs14 actions are best understood in the rodent brain, where it tonically suppresses synaptic plasticity and hippocampal-based learning (12, 13, 15), in the heart, where it diminishes myocardial remodeling (16), and in the brown adipose tissue metabolism linked to longevity (17). Much less is known about human RGS14. Human and rodent Rgs14 share a common domain structure, which includes an amino-terminal RGS domain that binds Gαi/o-GTP and acts as a GTPase-activating protein to limit G protein signaling (14, 18); two tandem Ras/Rap-binding domains that bind active H-Ras and Rap2 (19–21); and a G protein regulator (also referred to as GoLoco) motif that binds inactive Gαi1/3 to anchor Rgs14 at membranes (22). Human, primate, and ovine RGS14 differ from the rodent protein because they contain a carboxy-terminal class I PDZ-recognition sequence. Potential interaction and functional consequences of RGS14 engagement with PDZ proteins have not been described.

PDZ proteins, named for the common structural domain shared by the postsynaptic density protein 95 (PSD95), *Drosophila* disc large tumor suppressor (DlgA), and zonula occludens 1 protein (ZO1), constitute a family of 200 to 300 members (23, 24). These adapter molecules transiently assemble a variety of membrane-associated proteins, including transporters, receptors, ion channels, and signaling molecules in short-lived functional units. PDZ modules consist of 80 to 90 amino acids forming a 3-dimensional globular domain that is composed of six β-sheets (βA–βF) and two α-helices (αA and αB) within the larger protein (23). Scaffolding proteins harboring PDZ domains may contain single or multiple PDZ modules and can also include other protein–protein interaction motifs (24). Class I PDZ ligands take the form Asp/Glu-Ser/Thr-X-Φ (D/E-S/T-X-Φ), where X is promiscuous and Φ is a hydrophobic residue. The human RGS14 PDZ-recognition sequence is -Asp-Ser-Ala-Leu (-DSAL).

NPT2A is expressed at luminal membranes of proximal kidney tubules, where it mediates the bulk of Pi absorption from the urine (25). NPT2A activity is regulated by PTH and FGF23 and requires NHERF1 (26, 27). NPT2A also contains a carboxy-terminal PDZ motif that facilitates its binding to NHERF1 (28). NHERF1 possesses two tandem PDZ domains (PDZ1 and PDZ2) with identical core-binding sequences and a carboxy-terminal Ezrin-binding domain, through which interacting proteins are assembled at the plasma membrane and to cortical actin (29). Recent analysis disclosed that sites upstream of the PDZ-recognition sequence and the 3-dimensional organization of the PDZ module impart greater specificity to the recognition and binding determinants between the PDZ protein and the targeted partner (30).

Based on these considerations, we predicted that RGS14, acting through its PDZ ligand, binds NHERF1 and alters hormone-sensitive Pi transport. We theorized that human RGS14 genetic variants within the PDZ-binding motif might not share this behavior and, at the same time, afford further insight into the structural determinants for binding of the NHERF1 PDZ domains. The goal of the work here was to determine the effect of WT RGS14 and the identified PDZ ligand mutations on basal and hormone-regulated Pi transport and the role of RGS14 interactions with NHERF1 in this process. The described studies use a combination of native RGS14 expression in donor human kidney cells or immortalized kidney cell lines and engineered mutations and heterologous expression to demonstrate that RGS14 suppresses PTH and FGF23 actions of NPT2A by interacting with NHERF1.

[1] Human proteins are indicated by UniProt 3-letter uppercase abbreviation; genes are in italics. Only the first letter is uppercase for the corresponding rodent protein or gene.

Results

RGS14 blocks PTH-sensitive Pi uptake and colocalizes with NHERF1

We first explored the presence and localization of RGS14 along with the other protein components relevant to Pi uptake in the kidney. For this purpose, we employed unused donor human kidney tissue and prepared cultures of cells isolated from these samples. The goal was to define and characterize these proteins at spontaneous constitutive levels. RGS14 and NHERF1 are conspicuously expressed in human kidney (Fig. 1*A*). Protein lysates prepared from proximal tubule cells isolated from three independent patient samples (#55, #57, and #58) (Fig. 1*B*) displayed abundant RGS14 as well as NHERF1, NPT2A, and Ezrin, a proximal tubule cell marker that binds NHERF1 (31). RGS14 and NHERF1 coimmunoprecipitated in these samples expressing protein at endogenous levels (Fig. 1*B*). We next localized RGS14 in immortalized human proximal convoluted tubule (HPCT) cells and its binding to NHERF1. Proximity ligation assays (PLA) demonstrated the presence and significant colocalization of RGS14 with NHERF1, again at constitutive expression levels in HPCT cells (Fig. 1*C*).

We next examined the effects of RGS14 on PTH-sensitive Pi uptake cells derived from the donor samples. RGS14 (and RGS12) function as negative regulators of G protein signaling by inactivating Gα subunits. We reasoned that if RGS14 tonically inhibits PTH action, then ablating RGS14 should relieve this blockade. RGS14 siRNA knockdown (siRGS14) completely blocked RGS14 expression in primary kidney cells but did not affect actin expression (Fig. 2*A*). PTH did not inhibit Pi transport in these primary kidney cells (Fig. 2*B*), but siRGS14 conspicuously unmasked PTH-sensitive Pi transport (Fig. 2*B*). In HPCT cells, siRGS14 virtually eliminated RGS14 expression without detectably affecting protein levels of NHERF1, PTHR, or NPT2A (Fig. 2*C*). RGS14 siRNA knockdown revealed FGF23-sensitive and PTH-sensitive Pi transport (Fig. 2*D*). There was no hormone modulation of Pi transport in control cells transfected with scrambled siRNA. Treatment of HPCT cells with PF-06869206, a selective NPT2A inhibitor (32, 33), blocked phosphate uptake by greater than 95% (Fig. 2*D*), indicating that NPT2A mediates virtually all phosphate uptake by HPCT cells.

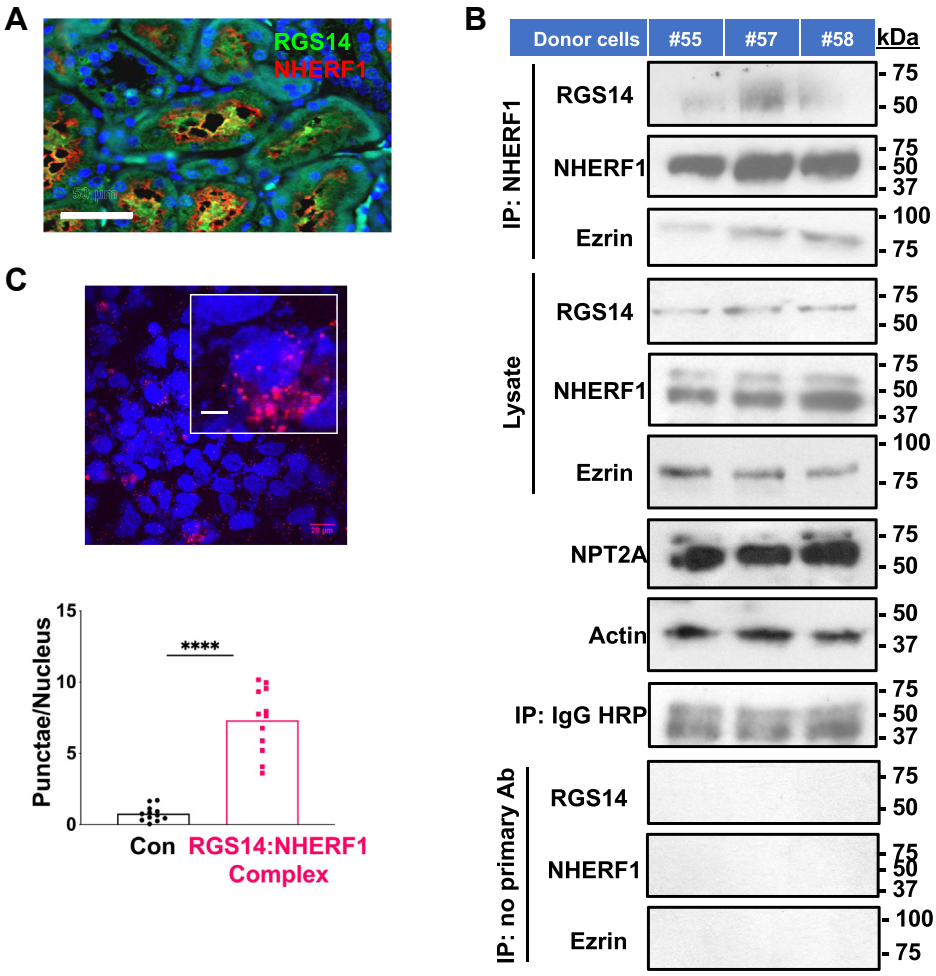

Figure 1. RGS14 and NHERF1 coexpress in human kidney cells and can be recovered as a stable complex. *A*, RGS14 and NHERF1 expression in human kidney. Representative image from whole-slide scan (40×) of formalin-fixed paraffin embedded 5-µm section of human kidney stained with RGS14 (*green*) and NHERF1 (*red*). The scale bar represents 50 µm. *B*, RGS14 immunoprecipitates with NHERF1 in proximal tubule cells. NHERF1 was immunoprecipitated from donor samples 55, 57, and 58. RGS14 and NHERF1 were analyzed as detailed in the Experimental procedures section. The result is illustrative of four experiments. In the absence of the primary anti-NHERF1 antibody, no bands were observed when RGS14, NHERF1, and Ezrin were immunoblotted (*bottom panels*). *C*, PLA characterization of the spontaneous interaction between RGS14 with NHERF1 in untreated HPCT cells. A representative 60× image and enlarged inset with scale bars of 20 µm are included. Technical details are described in the Experimental procedures section. A quantitative summary is shown in the accompanying graph (n = 4). ****$p < 0.001$, paired two-tailed *t* test. HPCT, human proximal convoluted tubule; NHERF1, sodium hydrogen exchanger regulatory factor-1; PLA, proximity ligation assay; RGS14, regulator of G protein signaling 14.

RGS14 actions on NPT2A are downstream of hormone receptor signaling

These findings suggested that RGS14 might directly interfere with PTHR signaling, thereby disrupting its physiological action on NPT2A. PTHR couples to Gs to stimulate cAMP production and activate PKA, which, in turn, phosphorylates NHERF1 to uncouple it from NPT2A (34–36). PTHR can also couple to Gq/11 (37, 38). RGS14 binds directly to active Gαi/o and inactive Gαi1/3 but does not directly engage either Gαs or Gαq (14, 39). We sought to determine if RGS14 affects PTHR G protein coupling and second messenger signaling directly or indirectly by binding NHERF1. Here, we applied live-cell bioluminescence resonance energy transfer (BRET) bimolecular fluorescence complementation assays using Ven-Gβ1γ2 and a mas-GRKct-Luc biosensor to detect Gβγ release (40, 41). Human embryonic kidney 293 (HEK293) cells were transfected with hemagglutinin (HA)-PTHR, Gsα, Gβγ-Ven, and GRK-Luc and either FLAG-RGS14 alone or NHERF1 plus FLAG-RGS14 (Fig. 3*A*). Cells were stimulated with PTH, activating PTHR, causing Gβγ-Ven dissociation from active Gαs, binding to GRK-Luc, and increasing the BRET signal as an index of G protein activation. The results show that RGS14 did not affect PTHR-G activation assessed as BRET from Gβγ-Ven and GRK-Luc (Fig. 3*B*). Consistent with this finding, RGS14 also did not alter PTH-triggered cAMP production. PTH stimulation of cAMP in cells transfected with the cAMP BRET sensor CAMYEL, PTHR, and either FLAG-RGS14 alone or NHERF1 plus RGS14 was not significantly altered in the presence of either RGS14 or NHERF1 alone, or when the two proteins were added in combination (Fig. 3*C*).

The absence of an effect of RGS14 on PTHR-Gs coupling or cAMP production suggested that RGS14 may exert its regulatory action at a postreceptor site. This interpretation predicts that RGS14 should interfere with PTH-PTHR and FGF23/FGFR1, regulation of Pi transport, and phosphorylate NHERF1

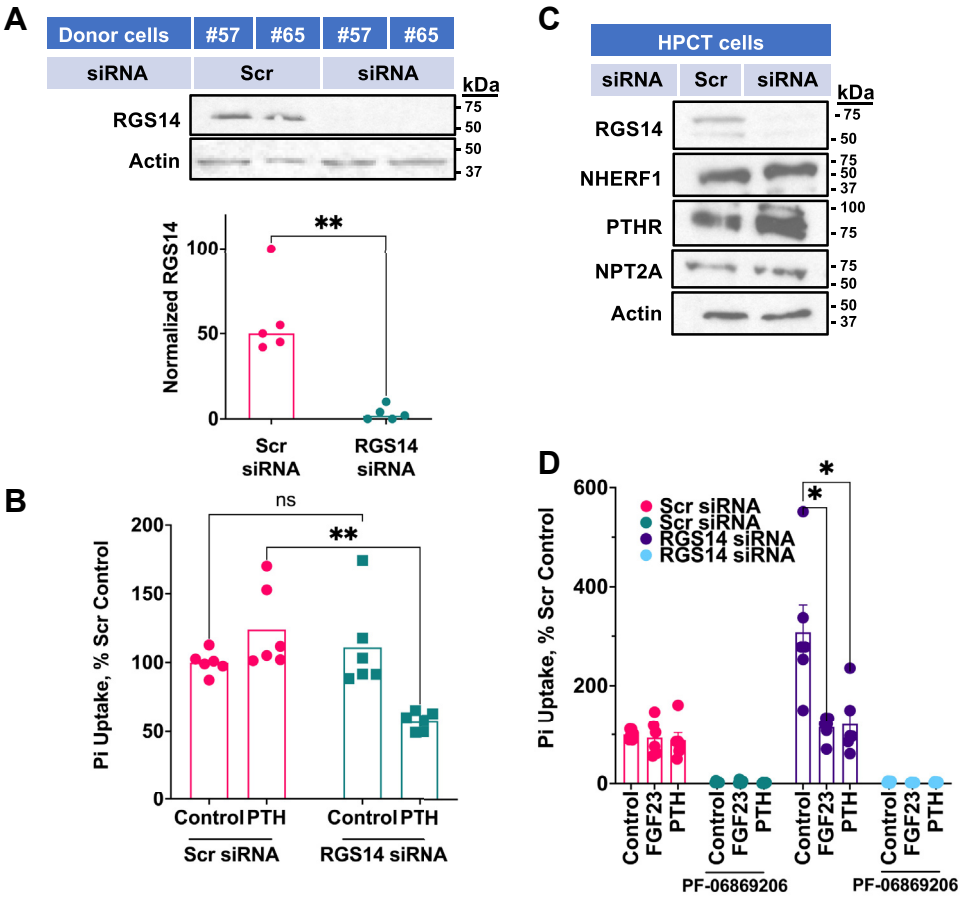

Figure 2. RGS14 knockdown unmasks PTH-sensitive phosphate uptake. *A*, siRNA ablation of RGS14 in primary human patient cells (*upper panel*, quantification normalized to actin in *lower panel*). Normalized RGS14 levels and statistical analysis of siRNA knockdown in six patient samples are depicted (paired two-tailed *t* test; $^{**}p < 0.0001$). *B*, siRNA knockdown of RGS14 unmasks PTH-sensitive Pi transport. Because patient samples gave comparable results with siRNA knockdown, they were combined to achieve sufficient material for transport experiments. Results were normalized for each experiment, where phosphate uptake under control untreated conditions was defined as 100%. Data represent the mean ± SE (error bars); n = 6 (two-way ANOVA with Bonferroni post hoc test; $F[1,10] = 15.84$, $p < 0.005$, $^{**}p < 0.001$). *C*, expression and siRNA knockdown on RGS14 in HPCT cells did not alter protein levels of other markers of phosphate transport. *D*, siRNA knockdown of RGS14 in HPCT cells reveals FGF23-sensitive and PTH-sensitive phosphate transport, mean ± SE; n = 6 (two-way ANOVA with Bonferroni post hoc test; $F[6,45] = 7.956$, $p < 0.0001$, $^{*}p < 0.0001$). One hundred micrometers PF-06869206 (PF) inhibited phosphate transport by greater than 95% (two-way ANOVA with Tukey's test for multiple comparisons ($F[10,15] = 4.030$, $p < 0.01$). FGF23, fibroblast growth factor 23; HPCT, human proximal convoluted tubule; PTH, parathyroid hormone; RGS14, regulator of G protein signaling 14.

dissociating it from NPT2A. To test this idea, we used human renal proximal tubule epithelial cells (RPTECs) that lack RGS14. Heterologous expression of RGS14 in RPTEC markedly obstructed PTH and FGF23 inhibition of Pi uptake (Fig. 4*A*), strongly suggesting that RGS14 acts at a common postreceptor locus of action shared by both PTH and FGF23 that directly engages the NPT2A–NHERF1 complex to regulate its function. Consistent with this view, FGF23 (and PTH) inhibited phosphate uptake in HPCT cells (Fig. 2*D*) supporting the idea that RGS14 actions are downstream of G proteins. When expressed in RPTEC, RGS14 was recovered by coimmunoprecipitation (IP) as a stable complex with NHERF1 and NPT2A (Fig. 4*B*). Together with findings from Figures 1 and 2, these observations establish that (1) RGS14 is expressed in human kidney and colocalizes with NHERF1; (2) RGS14 forms a stable complex with NHERF1; (3) RGS14 suppresses PTH- and FGF23-sensitive Pi transport; and (4) RGS14 knockdown unmasks hormone-regulated Pi transport. Thus, RGS14 inhibits PTH and FGF23 actions on NPT2A-mediated Pi uptake by engaging NHERF1.

RGS14 binds NHERF1

We next explored the molecular details by which human RGS14 and NHERF1 bind one another. Human RGS14 possesses a canonical class I carboxy-terminal PDZ ligand consisting of the sequence -DSAL (Fig. 5*A*) that is absent in rodent Rgs14. To confirm the requirement for the PDZ-recognition motif for binding with NHERF1, we generated constructs for full-length FLAG-tagged human hRGS14 and rat Rgs14 and performed co-IP experiments using HEK293 cells cotransfected with FLAG-RGS14/Rgs14 and HA-NHERF1. The results shown in Figure 5*B* substantiate that human RGS14 containing a PDZ ligand binds NHERF1, whereas rat Rgs14 lacking the PDZ ligand does not.

NHERF1 contains two tandem PDZ domains (Fig. 5*A*). The two NHERF1 PDZ domains share matching GYGF core-binding motifs but display substrate specificity that is not necessarily identical (42). We, therefore, inquired if RGS14 exhibited domain selectivity for binding with PDZ1 or PDZ2. For these experiments, we used NHERF1 constructs wherein the GYGF PDZ core-binding motif was mutated to GAGA in

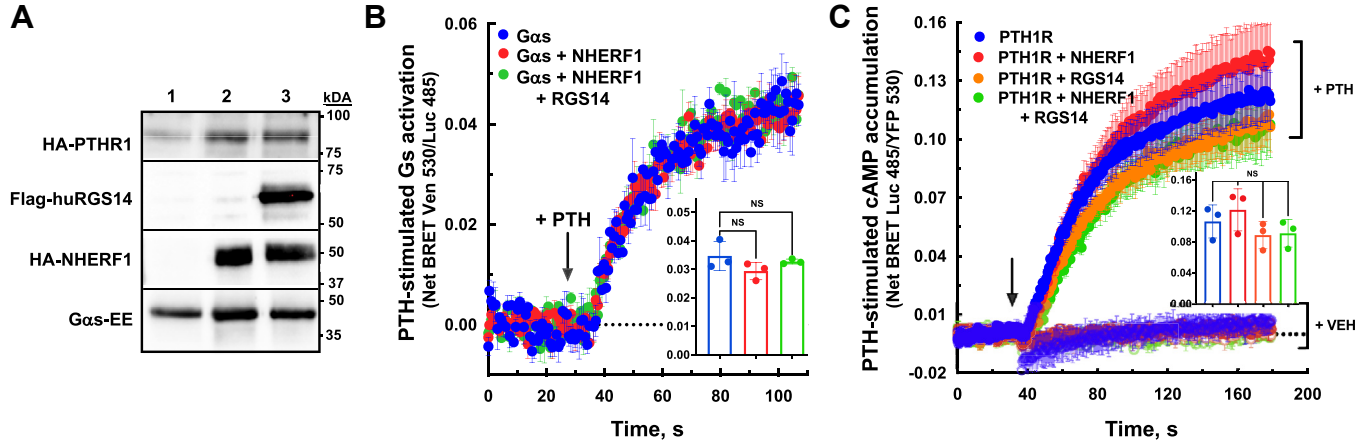

Figure 3. RGS14 and NHERF1 do not affect PTHR-Gαs coupling or cAMP formation. *A*, expression of proteins used in kinetic BRET studies. Technical details are provided in the Experimental procedures section. *B*, PTH–PTHR coupling to Gαs determined by BRET in live cells. Cells were treated with vehicle (ddH_2O) or 100 nM PTH(1–34) 30 s after measurements began. The hormone-stimulated BRET signal is measured as released Ven-Gβγ binding to membrane-associated mas-GRK3ct-Luc. *C*, PTH–PTHR-stimulated cAMP formation in live cells measured by BRET. HEK293 cells were transfected with cDNA encoding the cAMP BRET sensor CAMYEL and cotransfected with HA-PTHR alone or plus HA-NHERF1, FLAG-RGS14, or both HA-NHERF1 and FLAG-RGS14. About 48 h later, cells were treated with vehicle or 100 nM PTH(1–34) 40 s after initiating BRET measurement. The hormone-stimulated signal is measured as decreased BRET signal upon cAMP binding. Note that the BRET signal is inverted for simplicity. Data shown in *A* are representative of three separate experiments. Data presented in *B* and *C* are the pooled averages with SDs of n = 3. One-way ANOVA with Bartlett's test for multiple comparisons shown as figure insets was made at 60 s (*B*, $F[2,6] = 0.2421$, p = ns) and 120 s (*C*, $F[3,8] = 1.519$, p = ns). BRET, bioluminescence resonance energy transfer; cDNA, complementary DNA; ddH_2O, double-distilled water; HEK293, human embryonic kidney 293 cell line; NHERF1, sodium hydrogen exchanger regulatory factor-1; PTH, parathyroid hormone; PTHR, PTH G protein–coupled receptor; RGS14, regulator of G protein signaling 14.

PDZ1 (P1), PDZ2 (P2), or both domains (P1 and P2). As shown in Figure 5*C*, RGS14 binds to WT NHERF1 and NHERF1-P1 but not to NHERF1-P2 or the double mutant (P1P2), indicating that RGS14 selectively binds PDZ2 in cells. As a control, we confirmed that mutant NHERF1 P2 is functional (Fig. 5*D*) by showing that WT-NHERF1 and NHERF1 mutants P1 and P2 each bind Ezrin. Together, these findings indicate that the -DSAL PDZ ligand unique to human RGS14 selectively and directly binds to the PDZ2 domain of NHERF1.

Our findings suggest that human RGS14 binds directly to the PDZ protein NHERF1 (Fig. 5). To confirm this, we purified human RGS14, which contains a C-terminal PDZ-binding ligand, and rat RGS14, which lacks the PDZ-binding ligand. We then tested if either protein bound pure NHERF1 in an *in vitro* overlay dot blot assay (Fig. 6). Purified human and rat RGS14 were spotted onto nylon filters and allowed to dry (Fig. 6*A*). Then purified NHERF1 was incubated with the spotted membranes in an overlay assay to bind RGS14. Consistent with our results in cells (Fig. 5), we find that purified NHERF1 binds directly to purified human RGS14 but not rat Rgs14 which, notably, lacks the PDZ-binding motif (Fig. 6*A*). We next tested if purified full-length human NHERF1 carrying mutations in the PDZ core–binding sequence in either the PDZ1 (P1 null) or PDZ2 domain (P2 null) was able to bind human RGS14 (Fig. 6*B*). We find that P1 null human NHERF1 binds robustly to human RGS14, whereas P2 null also binds, but to a lesser extent. Together with findings in Figure 5, these findings suggest that RGS14 can bind both PDZ domains but prefers PDZ2.

Hormone-regulated renal Pi transport is mediated principally by NPT2A and requires NHERF1 (26, 43–46). PTH and FGF23 promote dissociation of NHERF1 from NPT2A (34–36, 47), and this action leads to the internalization of NPT2A and cessation of Pi uptake and absorption. As described above, RGS14 blocks PTH and FGF23 action on Pi transport. These findings raised the hypothesis that RGS14 stabilizes the NHERF1–NPT2A binary complex, accounting for or contributing to its mechanism of action. To test this idea, we performed co-IP experiments (Fig. 7) using host opossum kidney (OK) cells, the accepted standard model for PTH-regulated Pi transport studies (48). OK cells possess PTHR, FGFR1, NHERF1, and NPT2A, that is, all protein components except RGS14. They thus provide a null background on which to examine RGS14 actions. OK cells were transfected with FLAG-RGS14 or empty vector. As detailed in the Experimental procedures section, cells were treated with 100 nM PTH or FGF23 for 1 h. Figure 7*A* shows a representative example of four independent experiments. The results summarized in Figure 7*B* show that neither FGF23 nor PTH dissociates NHERF1 and NPT2A in the presence of RGS14, whereas in its absence, hormone treatment dissociates NPT2A from NHERF1. These observations are consistent with earlier results showing that FGF23 and PTH downregulate NPT2A (47) and are compatible with the conclusion that RGS14 stabilizes the NHERF1–NPT2A complex rendering it refractory to hormone-induced dissociation, presumably as a consequence of interfering with NHERF1 phosphorylation (36).

As noted previously, several GWASs implicate RGS14 in kidney disease. The linked mutations in those studies are in noncoding regions of the *RGS14* gene (5), suggesting they may alter protein expression levels. However, several rare coding region mutations are present in human RGS14, the PDZ-binding motif (9). Modifications are present at residues Asp^{563} and Ala^{565}, corresponding to positions -1 and -3 of the PDZ ligand. By convention, residues are numbered backward from zero at the carboxy terminus. The specific human

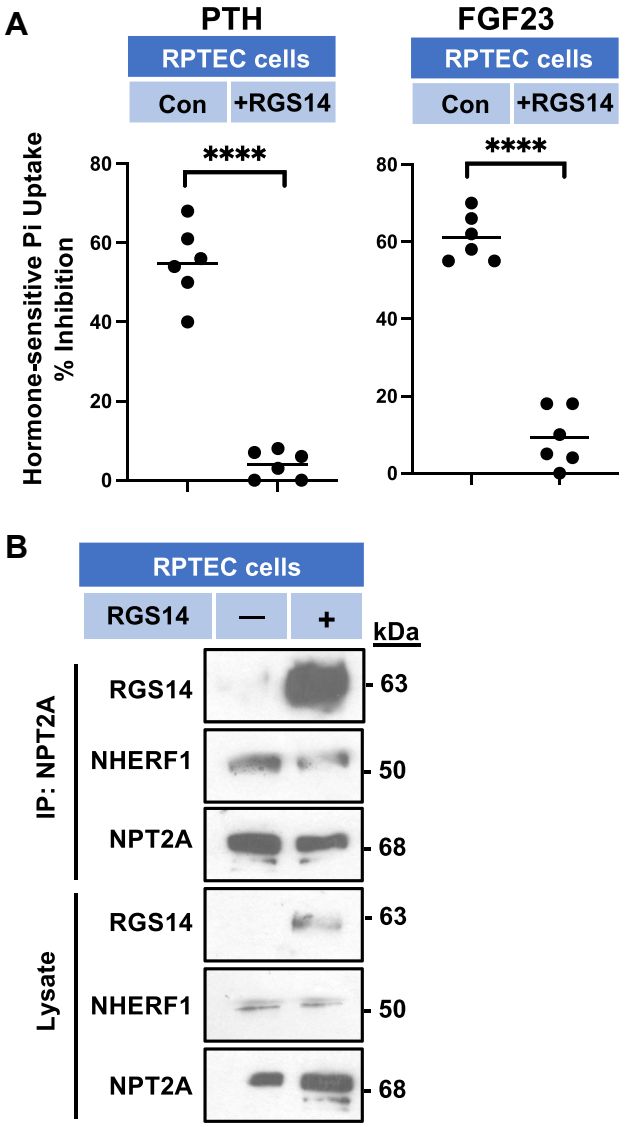

Figure 4. RGS14 suppresses hormone-regulated Pi transport. *A*, RGS14 inhibits PTH-sensitive and FGF23-sensitive phosphate uptake. Human RPTECs were transfected with empty vector (control) or human RGS14. After 48 h, cells were treated for 2 h with 10 nM PTH(1–34) or 100 nM FGF23. Phosphate uptake was measured as detailed in the Experimental procedures section. Data represent n = 6 independent experiments performed in triplicate. ****$p < 0.0001$ (paired *t* test). Data were normalized for each experiment, where phosphate uptake under untreated control conditions was defined as 0% inhibition. *B*, RGS14 forms a ternary complex with NHERF1 and NPT2A. RPTEC cells were transfected with HA-NPT2A, FLAG-NHERF1, and untagged hRGS14 as indicated. The NPT2A–NHERF1–RGS14 ternary complex was identified by serial immunoprecipitation (IP) of HA-NPT2A with agarose-conjugated monoclonal-anti-HA antibody, elution with 2 mg/ml HA peptide, followed by IP of FLAG-NHERF1 with subsequent immunodetection of RGS14. NPT2A was immunoprecipitated with agarose-conjugated monoclonal-anti-HA antibody, elution with 2 mg/ml HA peptide, followed by IP of FLAG-NHERF1 and subsequent detection of Ezrin by immunoblotting (*top three panels*). Input controls for each protein are shown in the *bottom three panels* (lysate). Duplicate experiments yielded identical results. FGF23, fibroblast growth factor 23; HA, hemagglutinin; NHERF1, sodium hydrogen exchanger regulatory factor-1; NPT2A, sodium phosphate cotransporter 2a; PTH, parathyroid hormone; RGS14, regulator of G protein signaling 14; RPTEC, renal proximal tubule epithelial cell.

variants are Asp^{563}Asn, Asp^{563}Gly, Ala^{565}Ser, and Ala^{565}Val. We summarize the normal sequence and the identified mutations in Figure 8*A*. These naturally occurring mutations provided a unique opportunity to characterize further the structural determinants of RGS14 binding to NHERF1. To delineate the consequence of these mutations on RGS14 binding to NHERF1 and their functional manifestations on Pi transport, we prepared the various modifications in the context of full-length FLAG-RGS14 (WT). WT-RGS14 or the indicated RGS14 mutant construct was cotransfected with HA-NHERF1 in HEK293 cells. Co-IP experiments were performed as described in the Experimental procedures section. Figure 8*B* (*left panel*, Asp^{563}X) is a representative immunoblot displaying the findings for WT (Asp) and RGS14 variants (Gly and Asn). The results show that substitution by Gly maintains the interaction with NHERF1, whereas replacement of Asp with Asn at residue 563 does not support binding to NHERF1.

We then turned our attention to Ala^{565} (Fig. 8*B*, *right panel*, Ala^{565}X). This residue corresponds to the promiscuous -1 position of the PDZ ligand (24) and hence should accommodate the reported Ser or Val variants. The results bear out this presumption, where both Val^{565} and Ser^{565} constructs avidly bound NHERF1.

These genetic variants provide a natural experiment that extends the present findings to characterize the structural determinants and their functional consequences for RGS14 binding to NHERF1. Besides the natural variants just described, we generated experimental mutations (Ala, Glu) at Asp^{563}. We predicted that by virtue of its greater length, Ala could not replace Asp but that Glu would substitute for Asp because of its charge. As shown in Figure 8*B*, Ala^{563} indeed failed to support interaction with NHERF1, as expected. Surprisingly, the Glu^{563} construct was unable to bind NHERF1 (Fig. 8, *A* and *B*).

We next wished to determine the effect of the various identified RGS14 coding-region mutations on basal and PTH-sensitive Pi transport (Fig. 8, *C* and *D*). For these studies, we again used OK cells as an RGS14-null model. Under control conditions, PTH inhibited Pi uptake by 60% in OK cells transfected with an empty vector (Fig. 8*C*). Hormone-sensitive Pi transport was abolished in cells transfected with WT Asp^{563} RGS14. The RGS14 Asp^{563}Gly mutant, like WT RGS14, bound NHERF1 and similarly eliminated PTH-dependent Pi transport. In contrast, the naturally occurring Asp^{563}Asn mutation disrupted this regulatory activity, as did the artificial mutations Asp^{563}Ala and Asp^{563}Glu (Fig. 8*C*). In contrast, the tolerated Ala^{565} variants at the permissive -1 position of the PDZ-recognition motif behaved like WT RGS14 and abolished PTH inhibition of Pi uptake (Fig. 8*D*). Notably, mutations that interfered with RGS14 binding to NHERF1 also hampered RGS14 capacity to affect PTH-regulated Pi transport. The data reveal a close correlation between RGS14 binding to NHERF1 and its ability to restrict PTH-sensitive Pi transport (Fig. 8*E*).

Computational modeling of RGS14 binding to NHERF1

RGS14 preferentially binds NHERF1 PDZ2 (Figs. 5*C* and 6*B*). Based on the structure/function findings outlined previously, we sought to understand better the structural parameters that dictate RGS14 binding to NHERF1. For this, we

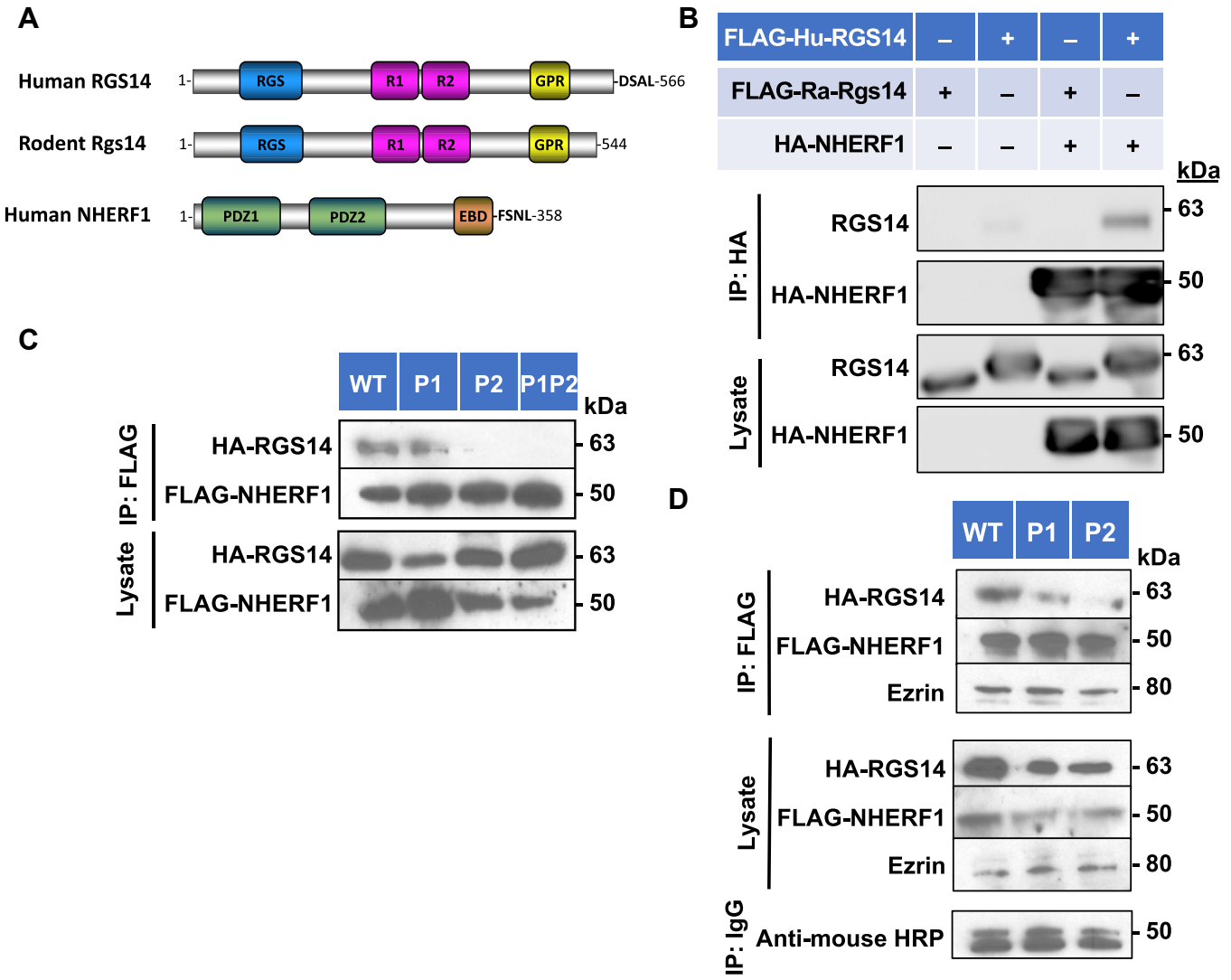

Figure 5. Human RGS14 interacts with NHERF1 in cells. *A*, schematic representation of human RGS14, rodent Rgs14, and human NHERF1 domain organization. PDZ ligands (DSAL and FSNL) are shown for human RGS14 and NHERF1. The location of the GYGF core–binding motif in NHERF1 PDZ1 and PDZ2 is indicated by the *blue vertical bars*. *B*, coimmunoprecipitation of human RGS14 with NHERF1. HEK293 cells were transfected with HA-rat Rgs14 or untagged human RGS14 with FLAG-NHERF1. Human RGS14 contains the PDZ ligand and binds NHERF1, whereas the rat RGS14 lacks the PDZ ligand and fails to interact with NHERF1, representative of n = 4. *C*, coimmunoprecipitation of RGS14 with WT NHERF1 and NHERF1 PDZ domain mutants. HEK293 cells were cotransfected with WT FLAG-NHERF1 or with constructs in which the GYGF core–binding motif was scrambled in PDZ1 (P1), PDZ2 (P2), or both PDZ1 and PDZ2 (P1P2) plus HA-RGS14. Each experiment was performed in duplicate with comparable results. *D*, control experiment showing the binding of Ezrin with NHERF1 mutants (P1 or P2). HEK293 cells were transfected with HA-RGS14 and either WT FLAG-NHERF1 or with constructs with scrambled PDZ1 (P1) or PDZ2 (P2) and recovered in complex with endogenous Ezrin as outlined in the Experimental procedures section. Loading controls are shown as recovered IG-heavy chain (IgG) blotted with HRP. Each experiment was performed three times with equivalent results. DSAL, Asp-Ser-Ala-Leu; HA, hemagglutinin; HEK293, human embryonic kidney 293 cell line; HRP, horseradish peroxidase; NHERF1, sodium hydrogen exchanger regulatory factor-1; RGS14, regulator of G protein signaling 14.

turned to molecular dynamic (MD) simulations (Fig. 9). Key residues involved in the binding of RGS14 and NHERF1 PDZ2 were evaluated using the 9-residue carboxy-terminal RGS14 peptide -^{558}Leu-Asn-Ser-Thr-Thr-Asp-Ser-Ala-Leu^{566} (-L^{-8}N^{-7}S^{-6}T^{-5}T^{-4}D^{-3}S^{-2}A^{-1}L^{0}; hereafter, referred to as RGS14ct-9) and explicit-solvent MD simulation. A representative structure of the PDZ2RGS14ct-9 complex after 150-ns MD simulation is shown in Fig. 9*A*. The structural stability for the complex was assessed by the RMSD over the backbone atoms of the PDZ2, RGS14ct-9 peptide, and complex. The RMSD values stabilized after approximately 50 ns (not shown). The average RMSD values along the last 20 ns of MD trajectory are 2.1 ± 0.1 Å, 1.7 ± 0.1 Å, and 1.8 ± 0.1 Å for the complex, PDZ2, and RGS14ct-9, respectively. These relatively small values indicate that the resulting complex is structurally stable during the MD simulations. Visual analysis of the evaluated structures confirmed that the docking position of the carboxy-terminal RGS14ct-9 peptide is similar to that of other PDZ-ligand systems (30, 42, 49). The RGS14ct-9 carboxy terminus occupies the binding groove between the α2 helix and β2 sheet. In contrast, the carboxy-terminal Leu-0 engages deep in the hydrophobic-binding pocket making canonical interactions with the residues from the carboxylate-binding loop of PDZ2 (-^{163}GlyTyrGlyPhe^{166}-), α2 helix (Val^{216} and Arg^{220}), and β2

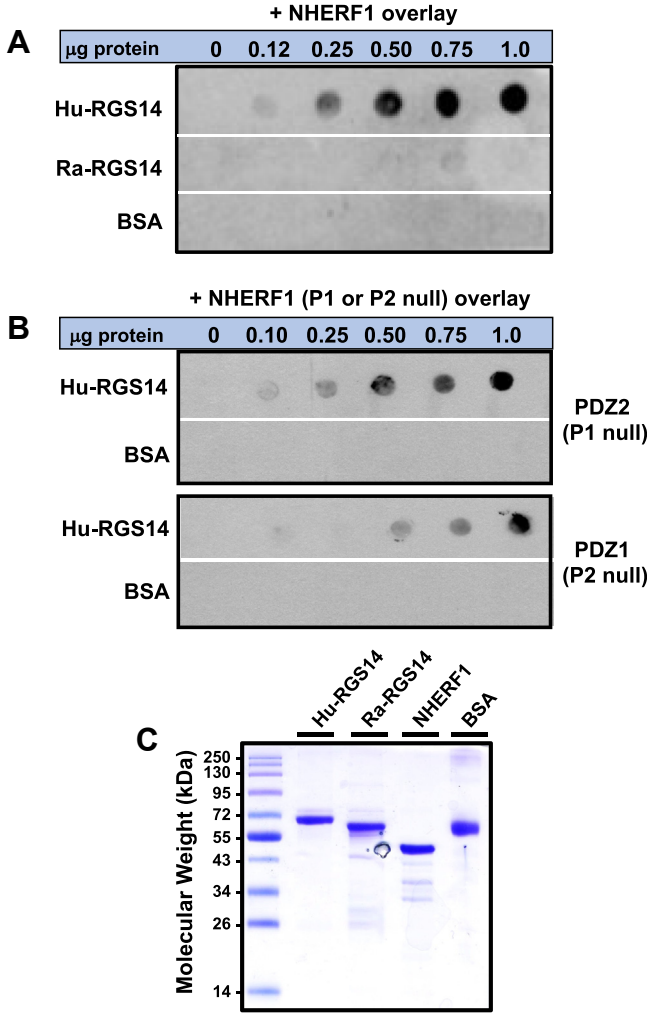

Figure 6. Recombinant human NHERF1 binds directly to human RGS14. *A*, overlay dot blot assay of NHERF1 binding to RGS14. Purified human RGS14, rat RGS14, and BSA protein control were spotted onto membrane filters at the indicated amounts and dried. Spotted membranes were incubated with purified human NHERF1, and, after washing, bound protein was detected by anti-NHERF1 immunoblot. *B*, overlay dot blot assays were repeated as aforementioned, except membranes were spotted with purified human RGS14 and BSA protein control. Spotted membranes were incubated with purified mutant forms of human NHERF1 harboring mutations within the PDZ core–binding motifs of each PDZ domain wherein the GYGF was mutated to loss-of-function GAGA in PDZ1 (P1 null) or PDZ2 (P2 null). Bound protein was detected by anti-NHERF1 immunoblot. *C*, Coomassie blue–stained SDS-page gel showing purified proteins used for overlay dot blots. Each blot is representative of three independent overlay experiments with similar results. BSA, bovine serum albumin; NHERF1, sodium hydrogen exchanger regulatory factor-1; RGS14, regulator of G protein signaling 14.

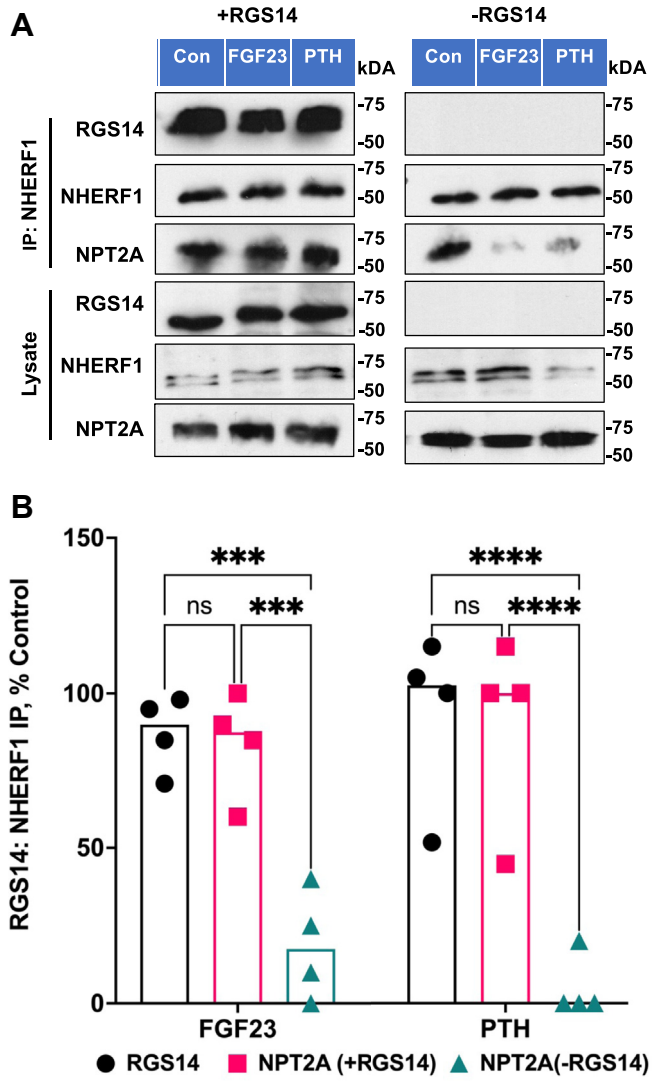

Figure 7. RGS14 stabilizes the NHERF1–NPT2A complex. OK cells were transfected with FLAG-RGS14 or empty vector. About 48 h later, cells were treated for 1 h with 100 nM PTH or FGF23, and NHERF1 was immunoprecipitated. The presence of NPT2A and RGS14 in the IP sample was analyzed by immunoblot. *A*, representative example of OK cells. *B*, summary of four independent experiments where the amount of RGS14 or NPT2A immunoprecipitating with NHERF1 is quantified. The data show that neither FGF23 nor PTH dissociates NHERF1 and NPT2A in the presence of RGS14, whereas in its absence, hormone treatment dissociates NPT2A from NHERF1 (two-way ANOVA with Bonferroni post hoc test $F[2,18] = 36.46$, $p < 0.0001$). ***$p < 0.001$ and ****$p < 0.00001$. FGF23, fibroblast growth factor 23; IP, immunoprecipitation; NHERF1, sodium hydrogen exchanger regulatory factor-1; NPT2A, sodium phosphate cotransporter 2a; OK, opossum kidney; PTH, parathyroid hormone; RGS14, regulator of G protein signaling 14.

sheet (Leu^{170}) similar to Leu-0 of the carboxy-terminal -Thr-Arg-Leu motif of G protein–coupled receptor kinase 6A (50). A second canonical interaction is formed between the OH group of Ser-2 of RGS14ct-9 and His^{212} of PDZ2. The distance between the carboxylate group of Asp-3 of RGS14ct-9 and the α-amino group of Arg^{180} or Asn^{169} of PDZ2 stabilizes between 2 and 6 Å with an average of 4.5 and 3.7 Å for the Asp-3 Oδ1 and Arg^{180} Nη22 and Asp-3 Oδ2 and Arg^{180} Nη12, respectively, and 4.6 Å for Asp-3 Oδ1 and Asn^{169} Nη21 (Fig. 8*A*). These ionic pairs may play a critical role in PDZ2–RGS14 association. In addition, the upstream Thr-4 of RGS14ct-9 is close enough to Gly^{170} of PDZ2 to form a backbone hydrogen bond.

Modeling of RGS14 coding variants

The RGS14 PDZ-recognition ligand binds in an extended groove of the PDZ domain between the second β-sheet (βB) and the second α-helix (αB) in an antiparallel fashion with the C-terminal hydrophobic amino acid of the ligand occupying the elongated hydrophobic cavity at the top of the binding groove. The binding to NHERF1 PDZ2 of the described RGS14

A

Mutation Position	-3 (563)	-2 (564)	-1 (565)	0 (566)
Wild-type	Asp	Ser	Ala	Leu
D563G	Gly	Ser	Ala	Leu
D563N	Asn	Ser	Ala	Leu
A565S	Asp	Ser	Ser	Leu
A565V	Asp	Ser	Val	Leu

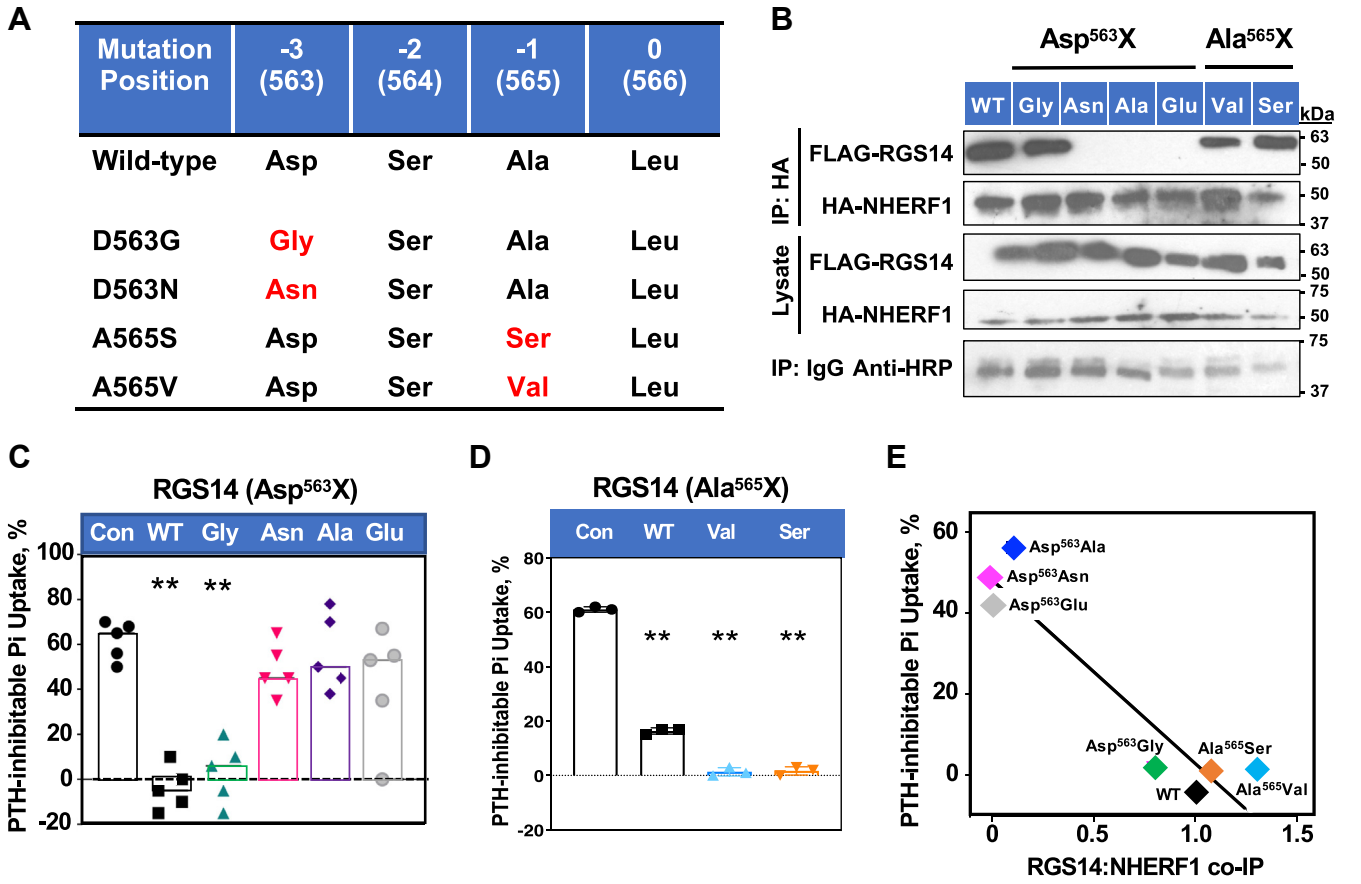

Figure 8. RGS14 genetic variants disrupt PTH-sensitive phosphate transport. *A*, tabular summary of naturally occurring human genetic variants of RGS14 at Asp^{563} and Ala^{565}. *B*, analysis of amino acid specificity at RGS14 Asp^{563} and Ala^{565}. Naturally occurring Asp^{563} variants (Asp^{563}Gly and Asp^{563}Asn) and artificial human RGS14 mutants (Asp^{563}Ala or Asp^{563}Gly). Coimmunoprecipitation experiments of NHERF1 binding to WT Asp RGS14 or with naturally occurring Gly or Asn variants. Asn at position 563 interrupted RGS14 binding to NHERF1, whereas Asp and Gly supported binding with NHERF1. Similar results were observed in n = 4 to 6 independent experiments. At the permissive -1 (565) position, the normally occurring Ala could be substituted by the two variant forms Val or Ser and robustly coimmunoprecipitated with NHERF1. *C* and *D*, phosphate transport in NHERF1-null opossum kidney (OKH) cells transfected with empty vector (control), WT NHERF1 (WT), or the indicated mutations at Asp^{563} (Asp^{563}Gly, Asp^{563}Asn, Asp^{563}Ala, or Asp^{563}Glu) or at Ala^{565} (Ala^{565}Val and Ala^{565}Ser) within the human RGS14 sequence. Measurements were performed in triplicate. n = 3 to 5 independent determinations. $^{**}p < 0.0001$ (*C*: one-way ANOVA with Dunnett post hoc test, $F[7,28] = 17.47$, $p < 0.0001$; *D*: one-way ANOVA with Dunnett post hoc test, $F[3,8] = 1359$, $p < 0.0001$). *E*, correlation analysis of PTH-inhibitable phosphate uptake as a function of RGS14 coimmunoprecipitation with NHERF1. $R^2 = 0.8896$. NHERF1, sodium hydrogen exchanger regulatory factor-1; PTH, parathyroid hormone; RGS14, regulator of G protein signaling 14.

mutations (Asp^{563}Asn, Asp^{563}Gly, Asp^{563}Ala, and Asp^{563}Glu) was tested using MD simulation with WT or mutant carboxy-terminal peptides (Fig. 9*B*). The WT PDZ2–RGS14ct-9 complex was used as a template to construct a model for each mutant, where Asp-3 in RGS14ct-9 was replaced iteratively by Asn, Gly, Ala, or Glu. Canonical PDZ–ligand interactions occur when a short length of three to four residues (β-strand) at the carboxy terminus of the target peptide occupies the PDZ-binding site. Therefore, WT RGS14ct-9 peptide or mutated variants were modeled as linear peptides bound to PDZ2. MD trajectories of 70 ns were prepared for each mutated complex except for the Gly mutant that was generated for 150 ns (for details, see the Experimental procedures section). A standard PDZ domain topology was observed for all structures, with the carboxy-terminal binding motif positioned in an extended position between the αB helix and βB sheet of PDZ2. Despite the residue differences at position -3 of the carboxy-terminal motifs (Fig. 8*A*), we did not observe significant deviations from the naturally occurring Asp. Contrary to what we expected from the results on Pi transport (Fig. 8*C*), we observed that RGS14ct-9Asn, RGS14ct-9Ala, and RGS14ct-9Glu participate in forming canonical contacts specific for class I motifs: -D/E-S/T-X-Φ. We surmise that substitution by Asn, Ala, Gly, or Glu at Asp-3 induces conformational changes or promotes the formation of local secondary structure at the carboxy-terminal motif of RGS14, thus, preventing association with the PDZ2 domain.

To test this theory, we applied PEP-FOLD3 (51) to predict the structure of a longer 23-amino acid carboxy-terminal fragment of WT RGS14 and the corresponding mutants (Fig. 9*B*) to discern conformational features that are difficult to observe with a short peptide. The five best models for WT and mutated peptides were acquired and viewed using PyMol (Molecular Graphics System, version 2.0; Schrödinger, LLC). Representative structures of the peptides are shown in Figure 9*B*. As can be seen, replacing Asp-3 by Asn, Ala, or Glu promotes the formation of a helical motif at the carboxy terminus, whereas the peptide with Gly favors the unfolded

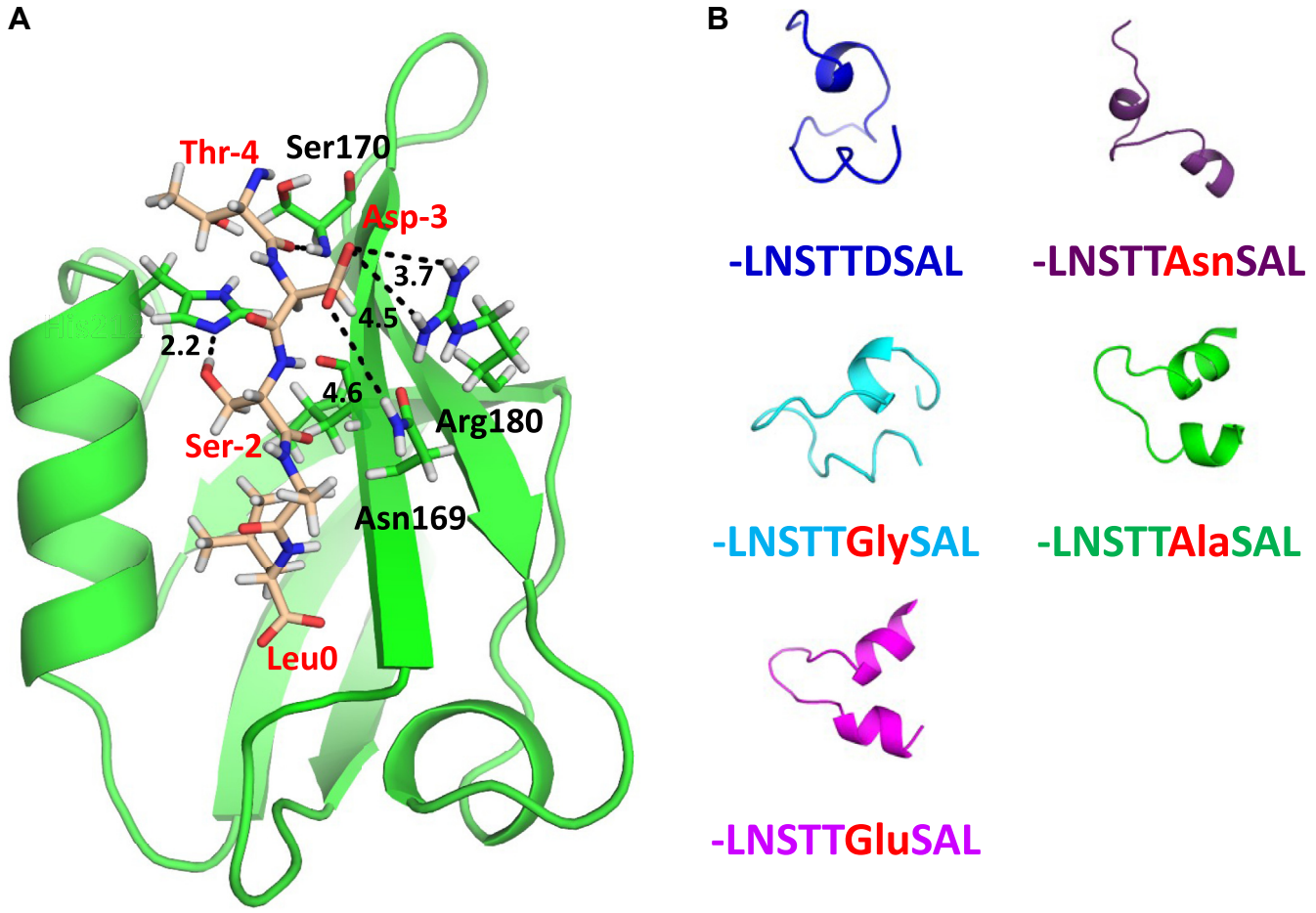

Figure 9. Computational prediction of NHERF1 PDZ2 binding to RGS14 and modeling of RGS14-coding variants. *A*, PDZ2 model structure showing bound carboxy-terminal RGS14ct-9 peptide. PDZ2 is highlighted in *green*, and the RGS14ct-9 peptide is represented as *wheat-colored sticks*. The key residues (except carboxy-terminal motif) stabilizing the complex are highlighted and labeled. The *dotted line* represents a hydrogen bond or salt bridge between a hydrogen atom and acceptor with the distance noted in Å. Hydrogen atoms are *white*, oxygens are *red*, and nitrogens are *blue*. *B*, representative structures of the 23-amino acid carboxy-terminal WT and indicated RGS14 variants. The structures of the unbound 23-residue peptide of RGS14 with Asn, Gly, Ala, or Glu at position -3 (*purple*, *cyan*, *green*, and *magenta*, respectively) tend to form a helical segment at the carboxy terminus, whereas a peptide with the Gly substitution (*cyan*) has a similar fold as WT RGS14 (*blue*). The structures were generated using the Pep-FOLD3 computational framework. NHERF1, sodium hydrogen exchanger regulatory factor-1; RGS14, regulator of G protein signaling 14.

conformation over the helical conformation. These findings provide provisional support for the concept that conformational changes promote dynamic secondary structure formation at the carboxy-terminal motif of RGS14 and serve as a starting point for further investigation and refinement.

Discussion

RGS14 in human kidney

The work described here had its origin in a GWAS report that implicated five gene products, including RGS14, in kidney disease (2). What particularly caught our attention was the presence of a canonical PDZ-recognition ligand at the RGS14 carboxy terminus. The prominent role of the PDZ protein NHERF1 in controlling hormone-regulated renal Pi conservation suggested possible structural and functional links between human RGS14, NHERF1, and NPT2A-mediated Pi uptake. Human RGS14 contains a 22-amino acid carboxy-terminal extension terminating with a prototypical type I PDZ-binding motif absent in rodents and most other species. The difference arises from a UAG stop codon in rodent exon 15 that terminates mRNA translation. The corresponding primate codon is CAG, which encodes the Gln (Q) at position 546 of RGS14.

Although RGS14 has been studied extensively in the brain and, to a lesser extent, the heart, its presence or conjectured role in kidney Pi transport had not been studied. Our findings show for the first time that RGS14 is expressed in human kidneys and localized in proximal and distal tubule cells. NPT2A is found exclusively in proximal tubules (52), where NPT2A-directed Pi transport takes place. Hence, the presence of RGS14 in distal tubule cells presumably involves some unrelated or ancillary regulatory action. NHERF1, expressed in renal proximal tubule cells but not in distal tubule cells, directly regulates PTH-sensitive and FGF23-sensitive Pi uptake by NPT2A (46, 53, 54). NPT2A mediates hormone-sensitive renal phosphate transport. NPT2C, an SLC34A1 paralog expressed in the kidney, lacks a PDZ ligand, does not

bind NHERF1, and is not directly regulated by PTH or FGF23 (43, 55). Consistent with these observations, the selective NPT2A inhibitor PF-06869206 virtually eliminated basal and hormone-sensitive phosphate accumulation, supporting the view that NPT2A accounts for essentially all phosphate uptake by HPCT cells.

RGS14 and NHERF1 colocalize and interact in human kidney cells at constitutive expression levels, and the two proteins can be recovered as a stable complex, indicating a putative functional link. Both human proximal kidney cells and the HPCT cell line, which express endogenous RGS14, are notably refractory to PTH or FGF23 regulation of NPT2A-mediated Pi uptake. Remarkably, siRNA knockdown and elimination of RGS14 protein unmasks hormone sensitivity and restores PTH and FGF23 capacity to block NPT2A Pi uptake. These findings suggest that RGS14 confers a tonic inhibition of PTH and FGF23 actions in the human kidney. Consistent with this idea, we show that addback of RGS14 to proximal tubule kidney cells lacking RGS14 (human RPTEC or opossum OK cells) restores inhibition of hormone action on Pi uptake. Together, these findings provide compelling evidence that RGS14 plays a newly appreciated role in regulating hormone-sensitive Pi uptake in the human kidney. This apparent tonic inhibition strongly suggests that RGS14 is a tightly regulated on/off switch for PTH and FGF23 control of NPT2A-mediated Pi uptake.

Mechanism of RGS14 action

RGS14 is a scaffolding protein that binds many other signaling protein partners (*e.g.*, active Gαi/o and inactive Gαi1/3 (14, 18, 22), active H-Ras, and Rap2A (19, 21, 56), Ca^{2+}/calmodulin (57), and 14-3-3γ (58). We initially considered that upstream signaling events leading to binding one or more of these partners might serve as a regulatory on–off switch for RGS14 interactions with the NPT2A–NHERF1 and/or PTHR–NHERF1 complexes. RGS14 may exert its action at the level of the PTHR. PTH activation of PTHR stimulates Gs-cAMP-PKA signaling and phosphorylation of NHERF1, which, in turn, uncouples NHERF1 from NPT2A, thereby inhibiting Pi uptake (54). Like RGS14, the PTH receptor also contains a PDZ ligand that binds NHERF1 to stabilize membrane localization and promote linked G protein signaling (38, 59). We considered whether RGS14 might bind NHERF1 to uncouple it from the PTHR and block PTH signaling. RGS14, however, did not affect PTHR signaling irrespective of NHERF1 presence. Furthermore, RGS14 notably failed to arrest PTHR Gs activation or cAMP formation. Based on this finding, we speculated that the RGS14 regulatory action occurs at a postreceptor locus. This consideration raised the hypothesis that RGS14 would also interrupt FGFR1–FGF23 control of Pi uptake, and, indeed, this was observed. What then is the mechanism by which RGS14 acts?

RGS14 directly binds NHERF1 preferentially at PDZ2, whereas NPT2A binds PDZ1 (54). NPT2A binding to NHERF1 is required for hormone-regulated Pi transport (46, 54). We theorized that RGS14 binding to NHERF1 may impact the dynamic and reversible interaction with NPT2A, thereby inhibiting PTH and FGF23 function. Consistent with this idea, RGS14 is recovered as a stable complex with NPT2A and NHERF1 (Fig. 4*B*). Further investigation revealed that RGS14 stabilizes the NHERF1–NPT2A binary complex, preventing PTH and FGF23-induced complex dissociation.

RGS14 mutants underscore structural determinants of binding and function

Multiple GWAS implicate RGS14 in disordered Pi metabolism associated with chronic kidney disease (2–7). Most of the identified variants are located in noncoding *RGS14* regions. We identified four naturally occurring genetic variants in the RGS14 PDZ ligand (9). These include two at Asp^{563} (Asp^{563}Asn and Asp^{563}Gly) and two at Ala^{565} (Ala^{565}Ser and Ala^{565}Val). Of these, only Asp^{563}Asn disrupted RGS14 binding to NHERF1 and PTH-sensitive Pi uptake, indicating this variant is a loss-of-function mutation that likely would cause disease. Although these genetic variants are rare, the parent gnomAD database includes a mixture of exome sequences derived from healthy and nonhealthy populations (8). Thus, these individuals may represent sporadic cases of chronic kidney disease not captured by GWAS. These variants also serve as natural experimental tools to explore structure/function relationships between RGS14 and NHERF1.

Our initial results affirmed that RGS14 binds NHERF1 and, more specifically, to PDZ2. The general motif of a four-part type 1 PDZ ligand takes the form -D/E-S/T-X-Φ. The particular RSG14 ligand sequence is -Asp-Ser-Ala-Leu. We expected that Asn or Gly mutations at the obligate -3 position (Asp^{563}) would disrupt binding to NHERF1 (60). Indeed, Asn substitution abolished binding as anticipated, but Gly replacement was innocuous. Asn contains an amide group in place of one of the Asp carboxyl groups making Asp electroneutral. Gly, in contrast, is shorter and includes a proton as its side chain, giving it greater conformational flexibility. Thus, in this instance, Gly^{563} is permissive for binding to NHERF1.

A related challenge emerged when we examined experimental Ala and Glu substitutions at Asp^{563}. Here, we predicted that Ala could not replace the shorter Gly and that negatively charged Glu would be an acceptable surrogate for the naturally occurring and negatively charged Asp. This, too, turned out to be partially correct since Glu could not replace Asp, again, a difference of a single carbon group. Based on these structural constraints, we performed MD simulations to model the residue-specific interactions of the RGS14 PDZ ligand with NHERF1 PDZ2.

NHERF1 PDZ1 and PDZ2 domains display extensive similarity and share identical GYGF core–binding motifs. How, then, do we explain the observed selectivity of the RGS14 carboxy-terminal -Asp-Ser-Ala-Leu PDZ-recognition motif for PDZ2? The model we advance here suggests that in addition to the canonical RGS14 PDZ ligand interactions between Leu-0 and residues from the -^{163}GYGF^{166}- loop of PDZ2, and Ser-2 and His^{212}, Arg^{180} from the β3 strand and Asn^{169} from the β2 strand further stabilize the PDZ2–RGS14 complex. The

predicted electrostatic interactions are similar to the Arg^{40}/Arg^{180}–Glu-3 ionic pair observed for the association of PDZ1–PDZ2 with PTHR (42).

The function of the carboxy terminus of RGS14 is related to its flexibility and ability to occupy the binding pocket of the PDZ2 domain. Modeling the peptide with the Asp-3/Gly-3 substitution revealed that the peptide is structurally stable and remains in the conformation similar to the WT RGS14 carboxy-terminal motif.

We surmise that loss of the electrostatic interaction between Asp-3/Gly-3 and Arg^{180} promotes conformational changes upstream of ligand position -3. Thr-4 changes its position and orientation to maintain a hydrogen bond equivalent to the Asp-3–Arg^{180} interaction in WT PDZ2-RGS14ct-9. We propose that distinct conformational changes in the carboxy-terminal motif of RGS14 induced by the mutations, except Gly, which is tolerated, impede association between PDZ2 and RGS14. The role of Asp-3 is to support a dynamic network between average conformations of the RGS14 carboxy terminus and its ability to occupy the PDZ2-binding pocket and interact with NHERF1.

In summary, we report here that human RGS14 plays an essential role in hormone-regulated Pi transport by NPT2A. We propose a working model for RGS14 actions in human renal proximal tubule cells (Fig. 10). NHERF1 forms a complex with NPT2A to stabilize the transporter at the apical membrane, thereby facilitating phosphate uptake. PTH and FGF23 block NPT2A phosphate uptake by phosphorylating NHERF1, resulting in disassembly of the NHERF1–NPT2A complex. Human RGS14 contains a PDZ motif that binds directly to NHERF1 to stabilize the NHERF1–NPT2A complex and oppose PTH and FGF23 actions (Fig. 10). This regulatory role of RGS14 involves direct and specific binding of its cognate PDZ ligand to the PDZ2 domain of NHERF1 (Figs. 5, 6, and 8). RGS14 imparts a tonic inhibition of PTH and FGF23 actions on Pi uptake that is reversed when RGS14 is removed in the human kidney. We determined the effects of identified human genetic variants within the RGS14 PDZ ligand on NHERF1 binding and found that (Asp^{563}Asn) disrupted the RGS14–NHERF1 complex and blocked RGS14 actions.

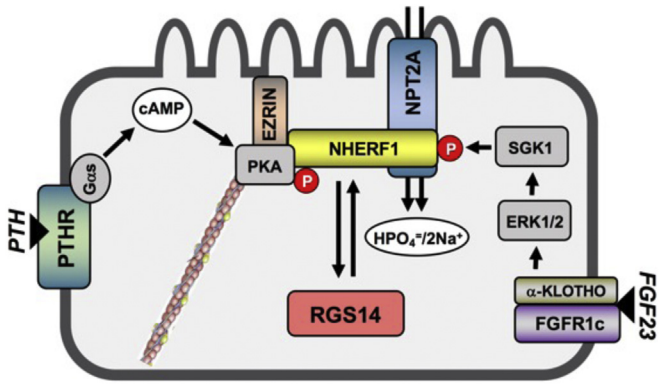

Figure 10. Working model for RGS14 regulation of hormone-sensitive phosphate uptake by human proximal tubule kidney cells. NHERF1 binding to NPT2A stabilizes the NHERF1–NPT2A complex at the plasma membrane to facilitate phosphate uptake. PTH and FGF23 each negatively regulate NPT2A phosphate uptake. PTH acting through the PTHR–Gs-cAMP–PKA pathway phosphorylates NHERF1 causing it to dissociate from NPT2A and block phosphate uptake. Similarly, FGF23 acting through the FGFR1c/αKLOTHO receptor–ERK–SGK1 pathway phosphorylates NHERF1 to uncouple it from NPT2A and also block phosphate uptake. Human RGS14, *via* its PDZ motif, binds directly to the PDZ2 domain of NHERF1 to stabilize the NHERF1–NPT2A complex, thus blocking PTH and FGF23 actions and inhibiting phosphate uptake. ERK, extracellular signal–regulated kinase; FGF23, fibroblast growth factor 23; NHERF1, sodium hydrogen exchanger regulatory factor-1; NPT2A, sodium phosphate cotransporter 2a; PTH, parathyroid hormone; RGS14, regulator of G protein signaling 14; SGK1, serum and glucocorticoid-regulated kinase 1.

The findings demonstrate a newly appreciated role for RGS14 in regulating Pi uptake in the kidney and identified at least one human genetic variant that blocks RGS14 actions. The results presented here demonstrate that RGS14 tonically impedes the phosphaturic actions of PTH and FGF23. This enigmatic observation begs several biological questions. What natural advantage accrues from persistent blockade of hormone action? PTH and FGF23 act with only a modest delay, so what triggers the release of RGS14 interdiction? This baseline negative regulatory activity may be a general feature of RGS14 since rodent Rgs14 inhibits specific hippocampal learning and memory formation (12). Why would a gene product exist that tonically inhibits several biological actions? As a start, we reasoned that a circulating factor could be released in response to elevated serum Pi just as FGF23 release is regulated in osteoblasts and osteocytes (61, 62). A released cofactor could phosphorylate RGS14, dissociating it from NHERF1, thus restoring hormone action to suppress NPT2A-mediated cellular phosphate uptake. Pilot experiments show that application of conditioned media from cultured human osteoblasts reestablishes PTH and FGF23 action on phosphate transport. If borne out, the findings suggest that resistance to hormone action in kidney failure and secondary hyperparathyroidism could arise from the curtailed release of the putative cofactor. Such a cofactor may impart an additional regulatory level of control of phosphate balance, at least in humans and other primates, where RGS14 contains a C-terminal extension with the PDZ-binding sequence. We note that though RGS14 action on the kidneys and Rgs14 effects on the brain share negative regulation, they involve different RGS14–Rgs14 structural features because the modulatory action of RGS14 on NPT2A-dependent phosphate transport depends on the RGS14 PDZ element, absent in rodent Rgs14 (Fig. 4). Future studies will further define novel signaling roles for RGS14 and the component functional modules in physiology and disease.

Experimental procedures

Chemical reagents, plasmids, and antibodies

Monoclonal anti-HA agarose (catalog no.: A2095) and rabbit polyclonal anti-FLAG (catalog no.: F7425) were purchased from MilliporeSigma. Rabbit polyclonal anti-HA (catalog no.: sc-805) and protein G+ agarose (catalog no.: sc-2002) were purchased from Santa Cruz Biotechnology. Mouse and rabbit polyclonal anti-NHERF1 antibodies were purchased from Abcam (catalog nos.: ab9526 and ab3452, respectively). Rabbit polyclonal anti-RGS14 was purchased from Proteintech (catalog no.: 16258-1-AP). We bought antihuman NPT2A

from Novus Biologicals (catalog no.: NBP242216) and anti-actin from Santa Cruz Biotechnology (catalog no.: sc-1616R). HA-NHERF1 as described (46). [Nle^{8,18},Tyr^{34}]PTH(1–34) was from Bachem (catalog no.: H9110). Recombinant human Arg^{179}Gln-FGF23$^{25–251}$ (referred to as FGF23), which is resistant to furin cleavage and inactivation, was obtained from R&D Systems (catalog no.: 2604-FG-025). PF-06869206 (catalog no.: PZ0389) was purchased from MilliporeSigma.

Human genetic variants and constructs

Human variants of RGS14 were acquired from the Genome Aggregation Database (GnomAD, version 2.0; Broad Institute) and filtered for missense variants. Four human variants were identified (Asp^{563}Gly and Asp5^{63}Asn and Ala^{565}Ser and Ala^{565}Val) and selected based on the change in side-chain properties. Reported minor allele frequencies for each variant are as follows: Asp^{563}Gly: global 0.0032% (0.0115% African); Asp^{563}Asn: global 0.0008% (0.003% Latino); Ala^{565}Ser: global 0.0004% (0.003% Latino); and Ala^{565}Val: global 0.0032% (0.007% European). Additional mutations were engineered (Asp^{563}Glu and Asp^{563}Ala) for structure/function analysis.

Mutations were added to FLAG-RGS14 using Qiagen QuikChange II and the following primers. *D563G*: (forward) GGA TCC TTG AAC TCC ACC GGC TCA GCC CTC; (reverse) GAG GGC TGA GCC GGT GGA GTT CAA GGA TCC. *D563N*: (forward) GGA TCC TTG AAC TCC ACC AAC TCA GCC CTC; (reverse) GAG GGC TGA GTT GGT GGA GTT CAA GGA TCC (reverse). *D563E* (forward) GGA TCC TTG AAC TCC ACC GAA TCC CCT CTG ACT CGA G; (reverse) CTC GAG TCA GAG GGC TGA TTC GGT GGA GTT CAA GGA TCC; *D563A*: (forward) GGA TCC TTG AAC TCC ACC GCC TCA GCC CTC TGA CTC GAG; (reverse) CTC GAG TCA GAG GCT GAG GCG GTG GAG TTC AAG GATCC. *A565S*: (forward): GAA CTC CAC CGA CTC AAG CCT CTG ACT CGA GTC TAG ATG; (reverse) CAT CTA GAC TCG AGT CAG AGG CTT GAG TCG GTG GAG TTC. *A565V*: (forward) GAA CTC CAC CGA CTC AGT CCT CTG ACT CGA GTC TAG ATG; (reverse) CAT CTA GAC TCG AGT CAG AGG ACT GAG TCG GTG GAG TTC.

Cell lines and culture

OK cells were obtained from J. Cole (63) and cultured in Dulbecco's modified Eagle's medium (DMEM)/F-12 (Corning; catalog no.: 10-090-CV) supplemented with 5% heat-inactivated fetal bovine serum (GenClone; catalog no.: 25-514H; Genesee Scientific) plus 1% penicillin and streptomycin. HEK293 cells were obtained from American Type Culture Collection. They were cultured in DMEM (Corning; catalog no.: 10-013-CV) supplemented with 10% fetal bovine serum plus 1% penicillin and streptomycin. Human RPTECs immortalized with human telomerase were obtained from American Type Culture Collection under license from Geron Corp. They were cultured in defined medium (DMEM/F-12 (Corning: catalog no.: 10-090-CV) supplemented with 5 PM triiodo-L-thyronine, 10 ng/ml recombinant human epidermal growth factor, 25 ng/ml prostaglandin E1, 3.5 μg/ml ascorbic acid, 1 mg/ml insulin, 0.55 mg/ml transferrin, 0.5 μg/ml sodium selenite, and 25 ng/ml hydrocortisone) plus 1% penicillin and streptomycin and 0.1 mg/ml of the selection antibiotic geneticin (G418).

HPCT-05-wt cells (hereafter, HPCT (64)) were obtained through Dr Ulrich Hopfer. HPCT cells were cultured in DMEM/F12 (Corning; catalog no.: 10-090-CV) supplemented with 10 ng/ml recombinant human epidermal growth factor, 3.5 μg/ml ascorbic acid, 1 mg/ml insulin, 0.55 mg/ml transferrin, 0.5 μg/ml sodium selenite, 25 ng/ml hydrocortisone, 5% heat-inactivated fetal bovine serum (GenClone; catalog no.: 25-514H; Genesee Scientific) plus 1% penicillin and streptomycin.

Tissue and cell preparation

Human adult kidney (HAK55, 63-year old male; HAK57, 53-year old male; and HAK58, 63-year old female); CD13 (proximal tubule), and CD227 (distal tubule) cells were from male and female donors, as indicated. Tissue procurement and processing have been described (65). CD13 and CD227 cells were seeded on 6-well plates. Lysates were prepared using 1% Nonidet P-40 buffer supplemented with protease inhibitor mixture I (EMD Millipore).

Protein lysates from mouse kidneys were prepared by mincing tissue with a razor blade on an ice-cold metal block. The minced kidney was then homogenized using a Cole-Parmer PTFE Tissue Grinder (30 ml) in 2 ml of ice-cold 1% Nonidet P-40 (50 mM Tris, 150 mM NaCl, 5 mM EDTA, and 1% Nonidet P-40) supplemented with protease inhibitor mixture I. After incubation on ice for 30 min, the lysate was centrifuged at 13,200 rpm in an Eppendorf 5415-R refrigerated microcentrifuge. The supernatant (mouse kidney protein lysate) was saved for immunoblot analysis. Animal studies were approved by the University of Pittsburgh Institutional Animal Care and Use Committee (protocol no.: 18073347).

Protein lysates were prepared from HEK293 cells transfected with RGS14. Cells were seeded on 6-well plates. About 24 h later, the cells were transfected with 1 μg/well of human RGS14 expression plasmid using jetPRIME (Polyplus). After 48 h, protein lysates were prepared using 1% Nonidet P-40 buffer supplemented with protease inhibitor mixture I.

Co-IP and immunoblotting

HEK293 cells were seeded on 6-well plates. About 24 h later, cells were transfected with 1 μg each/well of HA-NHERF1 and FLAG-RGS14 (WT, mutants as indicated) using jetPRIME. About 48 h post-transfection, cells were lysed with 1% Nonidet P-40 (50 mM Tris, 150 mM NaCl, 5 mM EDTA, and 1% Nonidet P-40) supplemented with protease inhibitor mixture I (EMD Millipore). Lysis was performed for 15 min on ice. NHERF1 was immunoprecipitated using anti-HA agarose overnight at 4 °C. IP samples were washed four times with 400 μl of lysis buffer and pelleted by spinning at 6000 rpm for 5 min at 4 °C in an Eppendorf 5415-R refrigerated microcentrifuge. The final pellet was resuspended in 60 μl of

SDS-PAGE sample supplemented with 5% β-mercaptoethanol (Sigma). Immunoprecipitated proteins were eluted by incubating samples for 5 min at 95 °C and then pelleting the agarose by spinning for 1 min at 13,200 rpm in an Eppendorf 5415 microcentrifuge. Supernatant proteins were resolved on 10% SDS-polyacrylamide gels and transferred to Immobilon-P membranes (Millipore) using the semidry method (Bio-Rad). Membranes were blocked for 1 h at room temperature with 5% nonfat dried milk in Tris-buffered saline plus Tween-20 (TBST) (blocking buffer) and incubated with the primary antibodies (polyclonal anti-FLAG at 1:1000 dilution, polyclonal anti-HA at 1:1000 dilution) in blocking buffer overnight at 4 °C. The membranes were washed four times for 10 min in TBST and then incubated with goat anti-rabbit immunoglobulin G conjugated to horseradish peroxidase at a 1:5000 dilution for 1 h at room temperature. Membranes were washed four times for 10 min in TBST. Protein bands were detected by Luminol-based enhanced chemiluminescence (EMD Millipore; catalog no.: WBKLS0500). Immunoblots were captured on film and quantified using ImageJ (imagej.nih.gov).

RGS14 knockdown

The Dicer-substrate siRNA duplex UUGAU-GUAUGAUA CUGUUAUUAUAA, UUAUAAUAACA-GUAUCAUACAUC AAGG, targeted to human RGS14, was designed and purchased from Integrated DNA Technologies.

HPCT cells were seeded on 6-well plates. About 24 h later, cells were transfected with 1 nM RGS14 siRNA or scrambled control. About 48 h post-transfection, cell lysates were prepared as described in the co-IP protocol.

Pi transport

Cells (RPTEC, OK, HPCT, or HEK) were seeded on 12-well plates. About 24 h later, where indicated, cells were transfected with 1 μg/well of WT or mutant FLAG-RGS14 plasmid, using jetPRIME. After 48 h, cells were serum-starved overnight and then treated for 2 h with 100 nM PTH(1–34) or FGF23, as specified. Pi uptake was measured as described (47). In experiments where NPT2A inhibition was examined, cells were preincubated with 100 μM PF-06869206 for 10 min before hormone addition. The hormone-supplemented medium was aspirated, and the wells were washed three times with 1 ml of sodium-replete wash buffer (140 mM NaCl, 4.8 mM KCl, 1.2 mM $MgSO_4$, 0.1 mM KH_2PO_4, 10 mM Hepes, pH 7.4). The cells were incubated with 1 μCi [^{32}P]orthophosphate (PerkinElmer Life Sciences; catalog no.: NEX053) in 1 ml of sodium-replete buffer for 10 min. Where indicated, 100 μM PF-06869206 was included in the Pi uptake assay buffer. Pi uptake was terminated by placing the plate on ice and rinsing the cells three times with sodium-free buffer (140 mM *N*-methyl-D-glucamine, 4.8 mM KCl, 1.2 mM $MgSO_4$, 0.1 mM KH_2PO_4, 10 mM Hepes, pH 7.4). The cells in each well were extracted overnight at 4 °C using 500 μl 1% Triton X-100 (Sigma). A 250-μl aliquot was counted in a Beckmann Coulter LS6500 scintillation spectrometer. Data were normalized to Pi uptake under control conditions defined as 100%.

Immunofluorescent staining and image capture

Immunofluorescent staining was performed with the PerkinElmer Opal kit (PerkinElmer). Briefly, thick formalin-fixed paraffin-embedded sections of 5-μm, baked and deparaffinized, were processed for antigen retrieval, blocking, primary and secondary antibody incubations, and signal amplification according to the manufacturer's protocol. RGS14 (catalog no.: 16258-1; Proteintech; 1:200 dilution) was visualized using Opal 520 (*green*), and NHERF1 (EBP50; catalog no.: ab3452; Abcam; 1:200 dilution) was visualized using Opal 570 (*red*).

Fluorescent images were acquired using the Aperio Versa Digital Pathology Scanner (Leica Biosystems). The Versa scanner is based on a Leica DM6000B microscope with motorized stage and autofocus capabilities. Slides were scanned at 40× objective magnification with the 4′,6-diamidino-2-phenylindole, FITC, and tetramethylrhodamine filters. Optimal exposure times were determined before automated scanning.

PLA

HPCT cells were maintained as described previously. PLAs were performed using the Duolink assay kit (Sigma). Cells were seeded on 22-mm diameter collagen-coated BioCoat German Glass coverslips (Corning; catalog no.: 354089). The experiments were performed when the cells reached confluence. The cells were washed three times with PBS and paraformaldehyde (paraformaldehyde 4% in PBS) added to each well for 15 min. Cells were rinsed three times again with PBS, and 100 mM glycine was added for 10 min to quench paraformaldehyde. The cells were permeabilized with 0.1% Triton X in PBS for 10 min and washed three times with PBS. Permeabilized cells were incubated with the following antibodies: mouse anti-NHERF1 (Abcam; catalog no.: ab9526) and rabbit anti-RGS14 (Abcam; catalog no.: ab96674). PLA probes were then added, and the assay was performed as per the manufacturer's instructions. Negative technical controls omitted the primary antibodies. Images were acquired in 14 z-planes, and PLA signals were normalized to the number of nuclei using Imaris software (Oxford Instruments). Results are expressed as the absolute number of PLA puncta per nucleus.

Kinetic BRET assays

HEK293 cells were cultured in 1× DMEM without phenol red and supplemented with 10% fetal bovine serum (5% for transfection medium), 2 mM L-Gln, 100 units/ml penicillin, and 100 mg/ml streptomycin. Cells were maintained in a humidified incubator with 5% CO_2 at 37 °C. Polyethyleneimine was used to carry out transfections. Cells were seeded 8×10^5 in 2 ml of transfection medium per well in 6-well plates. For PTHR Kinetic BRET, PTHR HEK293 cells were transfected with 200 ng 3× HA-PTHR, 1000 ng Gαs-Glu-Glu (short, (cDNA.org GNA0SSEIC0)), 200 ng Venus-Gβ1, 200 ng Venus-Gγ2, 200 ng, mas-GRK3ct-Luciferase, 200 ng HA-NHERF1, and 200 ng human-FLAG RGS14. To monitor intracellular concentrations of cAMP in live cells, we used the CAMYEL sensor (cAMP sensor using YFP-Epac-RLuc) as described (66).

HEK293 cells were transfected with 350 ng CAMYEL sensor, 500 ng 3× HA-PTHR, 250 ng HA-NHERF1, and 250 ng human-FLAG RGS14.

Kinetic BRET experiments were performed as previously described (67). About 48 h following transfection, cells were resuspended in Tyrode's solution (140 mM NaCl, 5 mM KCl, 1 mM $MgCl_2$, 1 mM $CaCl_2$, 0.37 mM NaH_2PO_4, 24 mM $NaHCO_3$, 10 mM Hepes, and 0.1% glucose, pH 7.4) and plated on white 96-well Optiplates (PerkinElmer Life Sciences). To confirm acceptor (YFP or Ven) expression, fluorescence measurements were made using the TriStar LB 941 plate reader (Berthold Technologies) with excitation of 485 nm and emission of 530 nm filters. After 2 min application of 5 μM coelenterazine H (Nanolight Technologies), kinetic BRET was monitored in live cells using sequential measurements through emission filters of 485 and 530 nm. BRET was recorded for 30 s with no stimulation to establish basal BRET. After basal BRET measurements, agonist PTH(1–34) (100 nM) was applied at 30 s. The change in BRET was calculated by dividing the mas-GRK3ct-Luc signal (530 nm) by the Ven-Gβγ signal (485 nm) and subtracting the average BRET signal observed from the first 30 s of observation (basal BRET). For each experiment, a kinetic BRET control was performed. For PTHR kinetic BRET, cells were treated with vehicle (double-distilled water), and any signal recorded in these controls was considered noise and subtracted from experimental kinetic BRET recording. For cAMP BRET experiments, cells were treated with vehicle, and the signal recorded in these controls was considered noise and plotted. Data were collected using MikroWin 2010 software (Mikrotek Laborsysteme GmbH) and analyzed using Microsoft Excel and GraphPad Prism 9 (GraphPad Software, Inc).

Overlay assays

Human RGS14 and rat Rgs14 were expressed as recombinant proteins in *Escherichia coli* and purified as previously described (68). Full-length human NHERF1 and NHERF1 mutants wherein the GYGF PDZ core–binding motif was substituted with GAGA in PDZ1 (P1 null) or PDZ2 (P2 null) were expressed as recombinant proteins in *E. coli* and purified as described (36, 42). For dot blot assays, purified human RGS14 and rat RGS14 were spotted on a nylon membrane and allowed to dry for 15 min. The membrane was then treated with pure NHERF1 or NHERF1 mutants at 5 mg/ml in a buffer in blocking buffer on a rocking incubator for 2 h at 4 °C. The membrane was then immunoblotted using an anti-NHERF1 primary antibody and anti-rabbit secondary (see the Experimental procedures section) to determine whether NHERF1 directly bound the RGS14 in the membrane.

System modeling and protocols for MD simulation and analysis

MD simulations were performed using the AMBER16 package with the AMBER force field (ff99SB). The model of NHERF1 PDZ2-bound carboxy-terminal fragment of RGS14 was prepared using the PDZ2–PTHR complex as a template (42). Using Leap (69), the nine-residue, carboxy-terminal -^{585}LeuGlnGluGluTrpGluThrValMet^{593} motif of PTHR was replaced by -^{558}LeuAsnSerThrThr-AspSerAlaLeu^{566} in RGS14. The complex was then solvated with TIP3P water molecules in a periodically replicated box, neutralized with a Na^+ ion, and energy minimized over 500 steps, including 100 steps of steepest descent minimization using the AMBER 16 pmemd module.

Equilibration and production simulations were performed as detailed previously (42). Briefly, the short runs (0.7–0.8 ns) were conducted under the NPT ensemble (constant number of particles [N], pressure [P], and temperature [T]) to equilibrate the water molecules. During equilibration, harmonic restraints were applied to the ligand and methodically lowered from k_s = 10 to 0.1 kcal/mol/Å^2. Then, equilibration runs (30–40 ns) were continued under the NVT ensemble with harmonic restrains k_s = 0.1 kcal/mol/Å^2 applied to the amino-terminal backbone atoms of the ligand and the PDZ domain. Production simulations (40–100 ns) were carried out with similar weak harmonic restrains (k_s = 0.1 kcal/mol/Å^2) to prevent diffusion of the complex from the simulation box. All simulations were performed at 300 K with configurations saved every 2 fs for analysis. The trajectories were analyzed with cpptraj, a complementary trajectory analysis program in the AMBER 16 suite. The RMSDs of the backbone atoms (N, CA, and C) relative to their starting positions were calculated for the PDZ2–RGS14 complex, PDZ2, and RGS14ct-9 over the entire MD trajectory. The absence of the backbone conformational changes for the core of PDZ2 and the carboxy-terminal motif of the bound peptide during the equilibration and production simulation indicates that the resulting complex is stable and remains close to the initial structure.

Statistical analysis

Results were analyzed using Prism 9 software. Data represent the mean ± SD or SEM as indicated of n ≥ 3 independent experiments and were compared by analysis of variance with post hoc testing using the Bonferonni procedure or paired *t* test as appropriate. *p* Values <0.05 were considered statistically significant.

Data availability

All described data are fully contained herein.

Acknowledgments—We acknowledge the Center for Organ Recovery and Education for providing human kidney tissue used here.

Author contributions—P. A. F. and J. R. H. conceptualization; T. M. methodology; W. B. S. and T. M. formal analysis; W. B. S., T. M., C. M.-M., S. R., N. H. H., K. E. S., J. V. G., and C. E. M. investigation; K. E. S. and D. R. E. resources; P. A. F. and J. R. H. writing–original draft; W. B. S., T. M., C. M.-M., and N. H. H. writing–review & editing; P. A. F. supervision; P. A. F. and J. R. H. funding acquisition.

Funding and additional information—This work was supported by the National Institutes of Health grants DK105811 (to P. A. F.); NS037112 and NS102652 (to J. R. H.); and GM140632-A1 (to J. R.

H. and P. A. F.). The content is solely the responsibility of the authors and does not necessarily represent the official views of the National Institutes of Health.

Conflict of interest—The authors declare that they have no conflicts of interest with the contents of this article.

Abbreviations—The abbreviations used are: BRET, bioluminescence resonance energy transfer; DMEM, Dulbecco's modified Eagle's medium; -DSAL, -Asp-Ser-Ala-Leu; FGF23, fibroblast growth factor 23; FGFR1, FGF receptor 1; GWAS, genome-wide association study; HA, hemagglutinin; HAK, human adult kidney; HEK293, human embryonic kidney 293 cell line; HPCT, human proximal convoluted tubule; IP, immunoprecipitation; MD, molecular dynamics; NHERF1, sodium hydrogen exchanger regulatory factor-1; NPT2A, sodium phosphate cotransporter 2a; OK, opossum kidney; PLA, proximity ligation assay; PTH, parathyroid hormone; PTHR, PTH G protein–coupled receptor; RGS14, regulator of G protein signaling 14; RPTEC, renal proximal tubule epithelial cell; TBST, Tris-buffered saline plus Tween-20.

References

1. Hernando, N., Gagnon, K. B., and Lederer, E. D. (2020) Phosphate transport in epithelial and nonepithelial tissue. *Physiol. Rev.* **101**, 1–35
2. Kestenbaum, B., Glazer, N. L., Kottgen, A., Felix, J. F., Hwang, S. J., Liu, Y., Lohman, K., Kritchevsky, S. B., Hausman, D. B., Petersen, A. K., Gieger, C., Ried, J. S., Meitinger, T., Strom, T. M., Wichmann, H. E., *et al.* (2010) Common genetic variants associate with serum phosphorus concentration. *J. Am. Soc. Nephrol.* **21**, 1223–1232
3. Urabe, Y., Tanikawa, C., Takahashi, A., Okada, Y., Morizono, T., Tsunoda, T., Kamatani, N., Kohri, K., Chayama, K., Kubo, M., Nakamura, Y., and Matsuda, K. (2012) A genome-wide association study of nephrolithiasis in the Japanese population identifies novel susceptible Loci at 5q35.3, 7p14.3, and 13q14.1. *PLoS Genet.* **8**, e1002541
4. Yasui, T., Okada, A., Urabe, Y., Usami, M., Mizuno, K., Kubota, Y., Tozawa, K., Sasaki, S., Higashi, Y., Sato, Y., Kubo, M., Nakamura, Y., Matsuda, K., and Kohri, K. (2013) A replication study for three nephrolithiasis loci at 5q35.3, 7p14.3 and 13q14.1 in the Japanese population. *J. Hum. Genet.* **58**, 588–593
5. Mahajan, A., Rodan, A. R., Le, T. H., Gaulton, K. J., Haessler, J., Stilp, A. M., Kamatani, Y., Zhu, G., Sofer, T., Puri, S., Schellinger, J. N., Chu, P. L., Cechova, S., van Zuydam, N., Consortium, S., *et al.* (2016) Trans-ethnic fine-mapping highlights kidney-function genes linked to salt sensitivity. *Am. J. Hum. Genet.* **99**, 636–646
6. Robinson-Cohen, C., Lutsey, P. L., Kleber, M. E., Nielson, C. M., Mitchell, B. D., Bis, J. C., Eny, K. M., Portas, L., Eriksson, J., Lorentzon, M., Koller, D. L., Milaneschi, Y., Teumer, A., Pilz, S., Nethander, M., *et al.* (2017) Genetic variants associated with circulating parathyroid hormone. *J. Am. Soc. Nephrol.* **28**, 1553–1565
7. Long, J., Chen, Y., Lin, H., Liao, M., Li, T., Tong, L., Wei, S., Xian, X., Zhu, J., Chen, J., Tian, J., Wang, Q., and Mo, Z. (2018) Significant association between RGS14 rs12654812 and nephrolithiasis risk among Guangxi population in China. *J. Clin. Lab. Anal.* **32**, e22435
8. Lek, M., Karczewski, K. J., Minikel, E. V., Samocha, K. E., Banks, E., Fennell, T., O'Donnell-Luria, A. H., Ware, J. S., Hill, A. J., Cummings, B. B., Tukiainen, T., Birnbaum, D. P., Kosmicki, J. A., Duncan, L. E., Estrada, K., *et al.* (2016) Analysis of protein-coding genetic variation in 60,706 humans. *Nature* **536**, 285–291
9. Squires, K. E., Montanez-Miranda, C., Pandya, R. R., Torres, M. P., and Hepler, J. R. (2018) Genetic analysis of rare human variants of regulators of g protein signaling proteins and their role in human physiology and disease. *Pharmacol. Rev.* **70**, 446–474
10. Hollinger, S., and Hepler, J. R. (2002) Cellular regulation of RGS proteins: Modulators and integrators of G protein signaling. *Pharmacol. Rev.* **54**, 527–559
11. Ross, E. M., and Wilkie, T. M. (2000) GTPase-activating proteins for heterotrimeric G proteins: regulators of G protein signaling (RGS) and RGS-like proteins. *Annu. Rev. Biochem.* **69**, 795–827
12. Evans, P. R., Dudek, S. M., and Hepler, J. R. (2015) Regulator of G Protein signaling 14: A molecular Brake on synaptic plasticity linked to learning and memory. *Prog. Mol. Biol. Transl. Sci.* **133**, 169–206
13. Evans, P. R., Gerber, K. J., Dammer, E. B., Duong, D. M., Goswami, D., Lustberg, D. J., Zou, J., Yang, J. J., Dudek, S. M., Griffin, P. R., Seyfried, N. T., and Hepler, J. R. (2018) Interactome analysis reveals regulator of G Protein signaling 14 (RGS14) is a novel calcium/calmodulin (Ca^{2+}/CaM) and CaM Kinase II (CaMKII) binding partner. *J. Proteome Res.* **17**, 1700–1711
14. Hollinger, S., Taylor, J. B., Goldman, E. H., and Hepler, J. R. (2001) RGS14 is a bifunctional regulator of $G\alpha_{i/o}$ activity that exists in multiple populations in brain. *J. Neurochem.* **79**, 941–949
15. Lee, S. E., Simons, S. B., Heldt, S. A., Zhao, M., Schroeder, J. P., Vellano, C. P., Cowan, D. P., Ramineni, S., Yates, C. K., Feng, Y., Smith, Y., Sweatt, J. D., Weinshenker, D., Ressler, K. J., Dudek, S. M., *et al.* (2010) RGS14 is a natural suppressor of both synaptic plasticity in CA2 neurons and hippocampal-based learning and memory. *Proc. Natl. Acad. Sci. U. S. A.* **107**, 16994–16998
16. Li, Y., Tang, X. H., Li, X. H., Dai, H. J., Miao, R. J., Cai, J. J., Huang, Z. J., Chen, A. F., Xing, X. W., Lu, Y., and Yuan, H. (2016) Regulator of G protein signalling 14 attenuates cardiac remodelling through the MEK-ERK1/2 signalling pathway. *Basic Res. Cardiol.* **111**, 47
17. Vatner, D. E., Zhang, J., Oydanich, M., Guers, J., Katsyuba, E., Yan, L., Sinclair, D., Auwerx, J., and Vatner, S. F. (2018) Enhanced longevity and metabolism by brown adipose tissue with disruption of the regulator of G protein signaling 14. *Aging Cell* **17**, e12751
18. Cho, H., Kozasa, T., Takekoshi, K., De Gunzburg, J., and Kehrl, J. H. (2000) RGS14, a GTPase-activating protein for Giα, attenuates Giα- and G13iα-mediated signaling pathways. *Mol. Pharmacol.* **58**, 569–576
19. Traver, S., Bidot, C., Spassky, N., Baltauss, T., De Tand, M. F., Thomas, J. L., Zalc, B., Janoueix-Lerosey, I., and Gunzburg, J. D. (2000) RGS14 is a novel Rap effector that preferentially regulates the GTPase activity of galphao. *Biochem. J.* **350 Pt 1**, 19–29
20. Willard, F. S., Willard, M. D., Kimple, A. J., Soundararajan, M., Oestreich, E. A., Li, X., Sowa, N. A., Kimple, R. J., Doyle, D. A., Der, C. J., Zylka, M. J., Snider, W. D., and Siderovski, D. P. (2009) Regulator of G-protein signaling 14 (RGS14) is a selective H-Ras effector. *PLoS One* **4**, e4884
21. Shu, F. J., Ramineni, S., and Hepler, J. R. (2010) RGS14 is a multifunctional scaffold that integrates G protein and Ras/Raf MAPkinase signalling pathways. *Cell. Signal.* **22**, 366–376
22. Shu, F. J., Ramineni, S., Amyot, W., and Hepler, J. R. (2007) Selective interactions between Giα1 and Giα3 and the GoLoco/GPR domain of RGS14 influence its dynamic subcellular localization. *Cell Signal.* **19**, 163–176
23. Hung, A. Y., and Sheng, M. (2002) PDZ domains: Structural modules for protein complex assembly. *J. Biol. Chem.* **277**, 5699–5702
24. Romero, G., Von Zastrow, M., and Friedman, P. A. (2011) Role of PDZ proteins in regulating trafficking, signaling, and function of GPCRs. Means, motif, and opportunity. *Adv. Pharmacol.* **62**, 279–314
25. Beck, L., Karaplis, A. C., Amizuka, N., Hewson, A. S., Ozawa, H., and Tenenhouse, H. S. (1998) Targeted inactivation of *Npt2* in mice leads to severe renal phosphate wasting, hypercalciuria, and skeletal abnormalities. *Proc. Natl. Acad. Sci. U. S. A.* **95**, 5372–5377
26. Cunningham, R., Xiaofei, E., Steplock, D., Shenolikar, S., and Weinman, E. J. (2005) Defective PTH regulation of sodium-dependent phosphate transport in NHERF-$1^{-/-}$ renal proximal tubule cells and wild-type cells adapted to low phosphate media. *Am. J. Physiol. Ren. Physiol.* **289**, F933–F938
27. Andrukhova, O., Zeitz, U., Goetz, R., Mohammadi, M., Lanske, B., and Erben, R. G. (2012) FGF23 acts directly on renal proximal tubules to induce phosphaturia through activation of the ERK1/2-SGK1 signaling pathway. *Bone* **51**, 621–628
28. Gisler, S. M., Stagljar, I., Traebert, M., Bacic, D., Biber, J., and Murer, H. (2001) Interaction of the type IIa Na/Pi cotransporter with PDZ proteins. *J. Biol. Chem.* **276**, 9206–9213

29. Brone, B., and Eggermont, J. (2005) PDZ proteins retain and regulate membrane transporters in polarized epithelial cell membranes. *Am. J. Physiol. Cell Physiol.* **288**, C20–C29
30. Mamonova, T., Zhang, Q., Khajeh, J. A., Bu, Z., Bisello, A., and Friedman, P. A. (2015) Canonical and noncanonical sites determine NPT2A binding selectivity to NHERF1 PDZ1. *PLoS One* **10**, e0129554
31. Reczek, D., and Bretscher, A. (1998) The carboxyl-terminal region of EBP50 binds to a site in the amino-terminal domain of Ezrin that is masked in the dormant molecule. *J. Biol. Chem.* **273**, 18452–18458
32. Filipski, K. J., Sammons, M. F., Bhattacharya, S. K., Panteleev, J., Brown, J. A., Loria, P. M., Boehm, M., Smith, A. C., Shavnya, A., Conn, E. L., Song, K., Weng, Y., Facemire, C., Juppner, H., and Clerin, V. (2018) Discovery of orally bioavailable selective inhibitors of the sodium-phosphate cotransporter NaPi2a (SLC34A1). *ACS Med. Chem. Lett.* **9**, 440–445
33. Clerin, V., Saito, H., Filipski, K. J., Nguyen, A. H., Garren, J., Kisucka, J., Reyes, M., and Juppner, H. (2020) Selective pharmacological inhibition of the sodium-dependent phosphate co-transporter NPT2a promotes phosphate excretion. *J. Clin. Invest.* **130**, 6510–6522
34. Zizak, M., Lamprecht, G., Steplock, D., Tariq, N., Shenolikar, S., Donowitz, M., Yun, C. H., and Weinman, E. J. (1999) cAMP-induced phosphorylation and inhibition of Na^+/H^+ exchanger 3 (NHE3) are dependent on the presence but not the phosphorylation of NHE regulatory factor. *J. Biol. Chem.* **274**, 24753–24758
35. Deliot, N., Hernando, N., Horst-Liu, Z., Gisler, S. M., Capuano, P., Wagner, C. A., Bacic, D., O'Brien, S., Biber, J., and Murer, H. (2005) Parathyroid hormone treatment induces dissociation of type IIa Na^+-P_i cotransporter-Na^+/H^+ exchanger regulatory factor-1 complexes. *Am. J. Physiol. Cell Physiol.* **289**, C159–C167
36. Zhang, Q., Xiao, K., Paredes, J. M., Mamonova, T., Sneddon, W. B., Liu, H., Wang, D., Li, S., McGarvey, J. C., Uehling, D., Al-awar, R., Joseph, B., Jean-Alphonse, F., Orte, A., and Friedman, P. A. (2019) Parathyroid hormone initiates dynamic NHERF1 phosphorylation cycling and conformational changes that regulate NPT2A-dependent phosphate transport. *J. Biol. Chem.* **294**, 4546–4571
37. Schwindinger, W. F., Fredericks, J., Watkins, L., Robinson, H., Bathon, J. M., Pines, M., Suva, L. J., and Levine, M. A. (1998) Coupling of the PTH/PTHrP receptor to multiple G-proteins. Direct demonstration of receptor activation of G_s, $G_{q/11}$, and $G_{i(1)}$ by [a-^{32}P]GTP-g-azidoanilide photoaffinity labeling. *Endocrine* **8**, 201–209
38. Wang, B., Ardura, J. A., Romero, G., Yang, Y., Hall, R. A., and Friedman, P. A. (2010) Na/H exchanger regulatory factors control PTH receptor signaling by differential activation of Gα protein subunits. *J. Biol. Chem.* **285**, 26976–26986
39. Vellano, C. P., Maher, E. M., Hepler, J. R., and Blumer, J. B. (2011) G protein-coupled receptors and resistance to inhibitors of cholinesterase-8A (Ric-8A) both regulate the regulator of g protein signaling 14 RGS14.Galphai1 complex in live cells. *J. Biol. Chem.* **286**, 38659–38669
40. Hollins, B., Kuravi, S., Digby, G. J., and Lambert, N. A. (2009) The c-terminus of GRK3 indicates rapid dissociation of G protein heterotrimers. *Cell Signal.* **21**, 1015–1021
41. Hynes, R. O. (2011) Metastatic cells will take any help they can get. *Cancer Cell* **20**, 689–690
42. Mamonova, T., Zhang, Q., Chandra, M., Collins, B. M., Sarfo, E., Bu, Z., Xiao, K., Bisello, A., and Friedman, P. A. (2017) Origins of PDZ binding specificity. A computational and experimental case study using NHERF1 and the parathyroid hormone receptor. *Biochemistry* **56**, 2584–2593
43. Christov, M., and Juppner, H. (2018) Phosphate homeostasis disorders. *Best Pract. Res. Clin. Endocrinol. Metab.* **32**, 685–706
44. Shenolikar, S., Voltz, J. W., Minkoff, C. M., Wade, J. B., and Weinman, E. J. (2002) Targeted disruption of the mouse NHERF-1 gene promotes internalization of proximal tubule sodium-phosphate cotransporter type IIa and renal phosphate wasting. *Proc. Natl. Acad. Sci. U. S. A.* **99**, 11470–11475
45. Mahon, M. J., Cole, J. A., Lederer, E. D., and Segre, G. V. (2003) Na^+/H^+ exchanger-regulatory factor 1 mediates Inhibition of phosphate transport by parathyroid hormone and second messengers by acting at multiple sites in opossum kidney cells. *Mol. Endocrinol.* **17**, 2355–2364
46. Wang, B., Means, C. K., Yang, Y., Mamonova, T., Bisello, A., Altschuler, D. L., Scott, J. D., and Friedman, P. A. (2012) Ezrin-anchored PKA coordinates phosphorylation-dependent disassembly of a NHERF1 ternary complex to regulate hormone-sensitive phosphate transport. *J. Biol. Chem.* **287**, 24148–24163
47. Sneddon, W. B., Ruiz, G. W., Gallo, L. I., Xiao, K., Zhang, Q., Rbaibi, Y., Weisz, O. A., Apodaca, G. L., and Friedman, P. A. (2016) Convergent signaling pathways regulate parathyroid hormone and fibroblast growth factor-23 action on NPT2A-mediated phosphate transport. *J. Biol. Chem.* **291**, 18632–18642
48. Biber, J., Malmström, K., Reshkin, S., and Murer, H. (1990) Phosphate transport in established renal epithelial cell lines. *Methods Enzymol.* **191**, 494–504
49. Karthikeyan, S., Leung, T., and Ladias, J. A. (2002) Structural determinants of the Na^+/H^+ exchanger regulatory factor interaction with the β_2 adrenergic and platelet-derived growth factor receptors. *J. Biol. Chem.* **277**, 18973–18978
50. Vistrup-Parry, M., Sneddon, W. B., Bach, S., Stromgaard, K., Friedman, P. A., and Mamonova, T. (2021) Multisite NHERF1 phosphorylation controls GRK6A regulation of hormone-sensitive phosphate transport. *J. Biol. Chem.* **296**, 100473
51. Lamiable, A., Thevenet, P., Rey, J., Vavrusa, M., Derreumaux, P., and Tuffery, P. (2016) PEP-FOLD3: Faster de novo structure prediction for linear peptides in solution and in complex. *Nucleic Acids Res.* **44**, W449–W454
52. Custer, M., Meier, F., Schlatter, E., Greger, R., Garcia-Perez, A., Biber, J., and Murer, H. (1993) Localization of NaPi-1, a Na-P_i cotransporter, in rabbit kidney proximal tubules–I. mRNA localization by reverse transcription/polymerase chain reaction. *Pflugers Arch.* **424**, 203–209
53. Weinman, E. J., Steplock, D., Shenolikar, S., and Biswas, R. (2011) Fibroblast growth factor-23-mediated inhibition of renal phosphate transport in mice requires sodium-hydrogen exchanger regulatory factor-1 (NHERF-1) and synergizes with parathyroid hormone. *J. Biol. Chem.* **286**, 37216–37221
54. Gattineni, J., and Friedman, P. A. (2015) Regulation of hormone-sensitive renal phosphate transport. *Vitam. Horm.* **98**, 249–306
55. Ho, B. B., and Bergwitz, C. (2021) FGF23 signalling and physiology. *J. Mol. Endocrinol.* **66**, R23–R32
56. Vellano, C. P., Brown, N. E., Blumer, J. B., and Hepler, J. R. (2013) Assembly and function of the regulator of G protein signaling 14 (RGS14). H-Ras signaling complex in live cells are regulated by Galphai1 and Galphai-linked G protein-coupled receptors. *J. Biol. Chem.* **288**, 3620–3631
57. Evans, P. R., Parra-Bueno, P., Smirnov, M. S., Lustberg, D. J., Dudek, S. M., Hepler, J. R., and Yasuda, R. (2018) RGS14 restricts plasticity in hippocampal CA2 by limiting postsynaptic calcium signaling. *eNeuro* **5**. https://doi.org/10.1523/ENEURO.0353-17.2018
58. Gerber, K. J., Squires, K. E., and Hepler, J. R. (2018) 14-3-3γ binds regulator of G protein signaling 14 (RGS14) at distinct sites to inhibit the RGS14:Gαi-AlF4$^-$ signaling complex and RGS14 nuclear localization. *J. Biol. Chem.* **293**, 14616–14631
59. Wang, B., Bisello, A., Yang, Y., Romero, G. G., and Friedman, P. A. (2007) NHERF1 regulates parathyroid hormone receptor membrane retention without affecting recycling. *J. Biol. Chem.* **282**, 36214–36222
60. Mamonova, T., and Friedman, P. A. (2021) Noncanonical sequences involving NHERF1 interaction with NPT2A govern hormone-regulated phosphate transport: Binding outside the box. *Int. J. Med. Sci.* **22**, 1087
61. Bonewald, L. F., and Wacker, M. J. (2013) FGF23 production by osteocytes. *Pediatr. Nephrol.* **28**, 563–568
62. Lang, F., Leibrock, C., Pandyra, A. A., Stournaras, C., Wagner, C. A., and Foller, M. (2018) Phosphate homeostasis, inflammation and the regulation of FGF-23. *Kidney Blood Press. Res.* **43**, 1742–1748
63. Cole, J. A., Forte, L. R., Krause, W. J., and Thorne, P. K. (1989) Clonal sublines that are morphologically and functionally distinct from parental OK cells. *Am. J. Physiol.* **256**, F672–F679
64. Orosz, D. E., Woost, P. G., Kolb, R. J., Finesilver, M. B., Jin, W., Frisa, P. S., Choo, C. K., Yau, C. F., Chan, K. W., Resnick, M. I., Douglas, J. G., Edwards, J. C., Jacobberger, J. W., and Hopfer, U. (2004) Growth,

immortalization, and differentiation potential of normal adult human proximal tubule cells. *In Vitro Cell. Dev. Biol. Anim.* **40**, 22–34
65. Emlet, D. R., Pastor-Soler, N., Marciszyn, A., Wen, X., Gomez, H., Humphries, W. H.t., Morrisroe, S., Volpe, J. K., and Kellum, J. A. (2017) Insulin-like growth factor binding protein 7 and tissue inhibitor of metalloproteinases-2: Differential expression and secretion in human kidney tubule cells. *Am. J. Physiol. Ren. Physiol.* **312**, F284–F296
66. Jiang, L. I., Collins, J., Davis, R., Lin, K. M., DeCamp, D., Roach, T., Hsueh, R., Rebres, R. A., Ross, E. M., Taussig, R., Fraser, I., and Sternweis, P. C. (2007) Use of a cAMP BRET sensor to characterize a novel regulation of cAMP by the sphingosine 1-phosphate/G13 pathway. *J. Biol. Chem.* **282**, 10576–10584
67. Brown, N. E., Lambert, N. A., and Hepler, J. R. (2016) RGS14 regulates the lifetime of Galpha-GTP signaling but does not prolong Gβγ signaling following receptor activation in live cells. *Pharmacol. Res. Perspect.* **4**, e00249
68. Brown, N. E., Goswami, D., Branch, M. R., Ramineni, S., Ortlund, E. A., Griffin, P. R., and Hepler, J. R. (2015) Integration of G protein α (Gα) signaling by the regulator of G protein signaling 14 (RGS14). *J. Biol. Chem.* **290**, 9037–9049
69. Case, D. A., Betz, R. M., Botello-Smith, W., Cerutti, D. S., Cheatham, T. E. I., Darden, T. A., Duke, R. E., Giese, T. J., Gohlke, H., Goetz, A. W., Homeyer, N., Izadi, S., Janowski, P., Kaus, J., Kovalenko, A., *et al.* (2016) *AMBER 16*, University of California, San Francisco